

DRAFT VERSION JULY 8, 2020
 Typeset using L^AT_EX **manuscript** style in AASTeX63

A search for rotation periods in 1000 *TESS* objects of interest

B. L. CANTO MARTINS,¹ R. L. GOMES,¹ Y. S. MESSIAS,¹ S. R. DE LIRA,¹ I. C. LEÃO,¹
 L. A. ALMEIDA,² M. A. TEIXEIRA,¹ M. L. DAS CHAGAS,³ J. P. BRAVO,¹ A. BEWKETU BELETE,¹ AND
 J. R. DE MEDEIROS¹

¹*Departamento de Física Teórica e Experimental, Universidade Federal do Rio Grande do Norte, Campus
 Universitário, Natal, RN, 59072-970, Brazil*

²*Departamento de Física, Universidade do Estado do Rio Grande do Norte, Campus Universitário Central, Mossoró,
 RN, 59610-090, Brazil*

³*Faculdade de Física/ Instituto de Ciências Exatas, Universidade Federal do Sul e Sudeste do Pará, 68505-080,
 Marabá PA, Brazil*

(Received May 2, 2020; Revised July 8, 2020; Accepted July 6, 2020)

Submitted to ApJS

ABSTRACT

The high quality light curves from the Transiting Exoplanet Survey Satellite (TESS) represent a unique laboratory for the study of stellar rotation, a fundamental observable driving stellar and planetary evolution, including planetary atmospheres and impacting on habitability conditions and the genesis of life around stars. As of April 14th 2020, this mission delivered public light curves for 1000 TESS Objects of Interest (TOIs), observed with 2 minute cadence during the first 20 months of the mission. Here, we present a search for rotation signatures in these TOIs, using Fast Fourier Transform, Lomb-Scargle, and wavelet techniques, accompanied by a rigorous visual inspection. This effort revealed 163 targets with rotation signatures, 131 of which present un-

Corresponding author: Bruno L. Canto Martins
 brunocanto@fisica.ufrn.br

ambiguous rotation periods ranging from 0.321 and 13.219 days, whereas 32 of them present dubious rotation periodicities. One hundred and nine of these stars show flux fluctuations whose root-cause is not clearly identified. For 714 TOIs, the light curves show a noisy behavior, corresponding to typically low-amplitude signals. Our analysis has also revealed 10 TOI stars with pulsation periodicities ranging from 0.049 to 2.995 days and four eclipsing binaries. With upcoming TESS data releases, our periodicity analysis will be expanded to almost all TOI stars, thereby contributing in defining criteria for follow-up strategy itself, and the study of star-planet interactions, surface dynamic of host stars and habitability conditions in planets, among other aspects. In this context, a living catalog is maintained on the Filtergraph visualization portal at the URL https://filtergraph.com/tess_rotation_tois.

Keywords: stars: rotation - stars: variables: general - stars: planetary systems - techniques: photometric

1. INTRODUCTION

Photometric space missions are revolutionizing our understanding of stellar periodicities, revealing a new view of the variability of stars in different regions of the HR Diagram. Thanks to the photometric observations carried out by the CoRoT (Baglin et al. 2009) and *Kepler* (Borucki et al. 2010) missions, different studies have revealed new insights on the rotation of main-sequence stars (e.g.; De Medeiros et al. 2013; Nielsen et al. 2013; Walkowicz & Basri 2013; McQuillan, Mazeh & Aigrain 2014; Leão et al. 2015; Paz-Chinchón et al. 2015; Davenport 2017; Reinhold & Hekker 2020), as well as in advanced stages of stellar evolution (e.g. Mosser et al. 2012; Van Saders & Pinsonneault 2013; De Medeiros et al. 2013; Costa et al. 2015). These works have shown that rotation is a major constraint in the study of the angular momentum, including the angular momentum transport from core to surface and expanding envelope in stars. The normalcy of the Sun's rotation with respect to the main-sequence stars with surface physical parameters close to solar values (De Freitas et al. 2013; Leão et al. 2015) and a bimodality in the rotation period distribution for M dwarf (McQuillan et al.

2013), K dwarf (McQuillan et al. 2014), and main-sequence stars with effective temperature above 5000 K (Davenport 2017) have also emerged from data acquired by the referred space missions. In addition, the observations of photometric modulation are also revealing traces of rotation in white dwarf stars, one of the scarce remaining clues of physics of the formation process of these stars (Maoz 2015, Kawaler 2015, de Lira et al. 2019).

The Transiting Exoplanet Survey Satellite (TESS) space mission (Ricker et al. 2015), launched into space in April 2018, is performing a 2-year nearly all-sky survey, during which differential time-series photometry are being acquired for hundreds of thousands of stars. Although the primary goal of TESS is to search for terrestrial planets transiting nearby bright stars, the large number of observed targets enables the study of other astrophysical phenomena, including stellar periodicities. For instance, first results based on TESS observations have revealed rapidly rotating M dwarfs with periods less than 1 day (Zhan et al. 2019), rotational and pulsation variability of magnetic chemically peculiar A-type stars (Cunha et al. 2019), and the identification of flares in M-type stars (Günther et al. 2019; 2020; Doyle et al. 2020).

The stellar environments in and around stars hosting planets are complex and unique laboratories for the understanding of the relation between the stars and orbiting companions. Much of the information about this interaction is encoded within their different variability phenomena, including rotation, pulsation and flares. Indeed, rotation is a paramount parameter driving the stellar evolution, playing also a major role in planetary evolution and habitability. The great significance of rotation is revealed by paralleling its role in the Solar System evolution, controlling the Sun's different transient phenomena, including radiative energy, the plasma outflow, shock waves, high-energy particle events during flares, and coronal mass ejections, which are key ingredients in the formation and atmospheric evolution of the planets including the terrestrial biosphere (e.g., Lundin et al. 2007; Lammer et al. 2012). In this context, the era of exoplanet transit surveys offers a unique possibility to the study of the rotation of stars hosting planets, thanks to the detection of quasi-periodic brightness variations in the photometric time series, caused by magnetically active regions crossing recurrently the visible hemisphere as the stars rotate (e.g., Irwin et al. 2009; Mc Quillan et al. 2014; Paz-Chinchón

et al. 2015). Deriving the rotation period for large samples of stars hosting planets has been a long-standing goal in stellar astronomy, with the potential to shed light on evolution of the angular-momentum of stars and their planetary system and to understand how magnetic features affect exoplanet parameters. For instance, intensive studies of the physical properties of the planets and their parent stars, including a possible star-planet interaction, have been conducted (Canto Martins et al. 2011; Miller et al. 2015; Viswanath et al. 2020). In addition, the advance in the knowledge of the rotation period of stars is also important in the support of exoplanet search, because stellar rotation may act itself on both photometric and spectroscopic data, preventing the detection and characterization of planets with orbital period near the stellar rotation period or its harmonics.

In this work we report a search for periodicities in the first 1000 TESS Objects of Interest (TOIs), mostly focused in the identification of rotation signatures, on the base of wavelet, Fast Fourier Transform and Lomb-Scargle analyses. Indeed, the philosophy of this effort is to offer for the exoplanet community, exploring TESS observations, a diagnostic of the presence of rotation phenomena in the TOI stars. As highlighted above, this work could provide valuable information to answer a large number of questions, including follow-up strategy itself, star-planet interactions, surface dynamic of host stars and habitability conditions in planets. The paper is organized as follows. Section 2 presents the data set used in our study and discusses the analysis procedure applied in the search for variability. Section 3 provides the main results. A summary is presented in Section 4.

2. STELLAR SAMPLE AND OBSERVATIONAL DATA

As underlined in the previous Section, TESS is an ongoing NASA photometric space mission and its main goal is the search for exoplanets by using the photometric transit method. In two years, the mission plan is to cover almost the entire sky by monitoring 26 segments (or sectors) of $90^\circ \times 24^\circ$, each one during 27 days. In the first and second years, the mission will complete the survey of the southern and northern ecliptic hemispheres, respectively. At higher ecliptic latitudes, there are overlap regions among the sectors where the targets can be observed for 54, 81, 108, 189, and 351 days. For a detailed description of the TESS mission see Ricker et al. (2015).

For the present purpose, we selected the first 1000 *TESS* Objects of Interest (TOIs) to perform a global search for periodicities using different procedures. *TESS* mission provides photometric data at two different cadences (2 and 30 minutes) with a time baseline from 27 days to 351 days, depending on sector overlap. While the 2-minute cadence data, also known as Target Pixel (TP) files, are available for a subset of targets, the entire CCDs, called full-frame images (FFIs), are binned on-board every 30 minutes and available via internet¹.

The *TESS* light curves (LCs) were automatically reduced and corrected for common instrumental systematics by the *TESS* data processing pipeline² (Jenkins et al. 2016). The *TESS* pipeline is based on that used by the *Kepler* Mission with further improvements. The data reduction performed by *TESS* is done using simple aperture photometry (SAP) on each TP files. The LCs for all targets are created and stored in arrays of fluxes. Subsequent detrend are applied to the LCs using the cotrending basis vectors, which represent the set of systematic trends present in the data for each CCD in each sector, and stored in other arrays called pre-search data conditioning (PCDSAP). In this study, we are using the 2-minute cadence PCDSAP data retrieved via Space Telescope at Science Institute Webpage³.

While the detection of periodicities in LCs is straightforward, their interpretation in terms of the root-causes is far a challenging task. Indeed, the detection threshold for periodicity it depends on star brightness, time span of observations, and the final cleaning of the LCs, varying thus from star to star. In this sense, to avoid possible distortions in the signature of periodicities, we have performed an additional treatment of outlier removal and instrumental trend correction for the LCs following the procedure by De Medeiros et al. (2013) and Paz-Chinchón et al. (2015). We performed such a treatment when needed plus a removal of transits in a similar way to that described in Paz-Chinchón et al. (2015). The reader is referred to those authors for a complete explanation on this post-treatment and data analysis, which is summarized below.

¹ <http://archive.stsci.edu/tess>

² <https://heasarc.gsfc.nasa.gov/docs/tess/pipeline.html>

³ http://archive.stsci.edu/tess/bulk_downloads/bulk_downloads_ffi-tp-lc-dv.html

In summary, our post-treatment consisted of removing eventual *flare-like*⁴ signatures from the PDCSAP LCs, as well as the known planetary transits based on the TOI catalog⁵. Nevertheless, those features were analyzed separately for identification of physical flares and binarity. A few jumps were corrected based on De Medeiros et al. (2013) and Bányai et al. (2013), by taking a linear fit and extrapolation of user-defined boxes before and after each jump. Individual LCs of each TESS sector were then detrended with third-order polynomial fits. This step is basically a high-pass filter that helps in suppressing long-term trends usually associated to instrumental systematics (e.g., Smith et al. 2012; Basri et al. 2011). Of course, such a filter may also suppress long-period physical variabilities, but in the present study such periods would be longer than the typical 28-day time span of the TESS sectors, namely a technical limit for period determination (e.g., Günther et al. 2020). Finally, removal of outliers was performed by excluding any flux measurement greater than $3.5 \times$ the standard deviation of the detrended LCs. In addition, individual LCs that were overlapped in multiple sectors were combined to produce a single long-term time series for each object. These steps produced rather clean LCs without transits (or flares) that allowed inspection of stellar variations such as rotational modulation.

2.1. Identifying periodicities

The post-processed LCs were analyzed by using three different periodicity analysis techniques, namely (i) Lomb-Scargle periodograms (e.g., Scargle 1982; Horne & Baliunas 1986; Press & Rybicki 1989), (ii) Fast Fourier Transform (FFT) (see Zhan et al. 2019 for details) and (iii) wavelet analysis (Grossmann & Morlet 1984). In fact, we consider these three methods to identify consistent periodicities. In general, these procedures can provide additional information to a visual inspection of the LCs. It is common that the peak powers in the power spectrum (or periodogram) of a method do not follow the same sequence of another method. Even in those cases, we interpret periodicities as far as they are revealed by different methods, and given that they are statistically confident. In

⁴ A noticeable flux bump typically of few hours, whose physical or instrumental origin was inspected separately.

⁵ <https://tess.mit.edu/toi-releases/>

particular, the Lomb-Scargle method is useful for validating periods according to their false alarm probabilities (FAPs; see Horne & Baliunas 1986), whereas the wavelet maps strongly help to interpret morphological nuances of periodic signatures (e.g., Bravo et al. 2014). We have considered a broad frequency range of $0.01\text{--}10.0 \text{ d}^{-1}$ to search for rotation and pulsation signatures. Those three methods are described shortly in Sects. 2.2, 2.3, and 2.4. The periods given in our catalog are those from the peaks of wavelet global spectra and their errors are computed using Eq. (2) of Lamm et al. (2004), being typically around 5%.

Different authors have described, in detail, rotational modulation as being a semi-sinusoidal variability associated to the dynamic behavior of star spots (e.g.: Basri & Nguyen 2018; Basri 2018; De Medeiros et al. 2013; Lanza et al. 2003, 2007). In short, that signature is characterized by semi-regular flux variations that used to be multi-sinusoidal, most commonly showing single or double dips per rotation cycle. The double-dip signature has been traditionally interpreted following a simplistic view of being caused by two main spots at opposite hemispheres (e.g.: Donnelly & Puga 1990; Lanza et al. 2009; Walkowicz et al. 2013; De Medeiros et al. 2013). However, based on Basri & Nguyen (2018) and Basri (2018), either single- or double-dip signatures are more likely an effect of hemispheric asymmetries caused by the presence of a few or several spots, their surface distribution and dynamics. Rotational modulation also often presents long-term amplitude variations associated to activity cycles (e.g.: Ferreira Lopes et al. 2015) that used to be somewhat irregular, as well as showing some asymmetry with respect to the flux average. On the other hand, pulsation typically displays a more regular shape of the flux variation and may have constant amplitude, or a regular amplitude variation usually forming steady beats (which can be clearly seen, in particular, in the wavelet maps). Some pulsators, such as for example Gamma Douradus variables, may present some irregularities in their LCs that can be confused with rotational modulation. Those cases can be disentangled when presenting an asymmetry in their variability signatures skewed to higher fluxes, differently of the rotational modulation that tends to present an asymmetry skewed to lower fluxes. A few cases are difficult to unravel, so an additional analysis considering the stellar physical parameters

is performed to identify their natures. When no conclusion can be taken for some cases, then an ambiguous variation is set to their LC classifications.

2.2. The Fast Fourier Transform Analysis

The Fast Fourier Transform (FFT), a computationally faster version of the Discrete Fourier Transform (DFT), is a discrete version of the continuous Fourier Transform that can decompose periodicities of real data. The algorithm used in this work is based on Cooley & Tukey (1965) and similar to the one employed by Sanchis-Ojeda et al. (2013, 2014), but is optimized for the TESS data. The main advantage of FFT is its computational speed, which is not a requirement for our purposes because our sample is not too large. We simply use FFT as a complementary method for interpreting periodicities. As a limitation, FFT is applicable for evenly-sampled time series. The TESS LCs are nearly evenly sampled with a few irregularities, especially when having some gaps. To ensure that the LCs are evenly spaced, we rebinned the data to regular time intervals close to their original bins and fulfilled eventual gaps with linear interpolation.

2.3. The Lomb-Scargle Analysis

Lomb-Scargle (Lomb 1976; Scargle 1982) is a well-known algorithm that can provide Fourier-like periodograms of real (discrete) data. Its main advantage over FFT is the fact that it can deal with unevenly-sampled time series. Periodograms can thus be obtained directly from the LCs with their original time samplings, without the need of any rebinning or interpolation. Another useful feature, developed by Horne & Baliunas (1986), is a formal calculation, inherent to the method, of false alarm probabilities (FAP) for detected periods. Such a statistics helps us in quantitatively validating periods. Stellar variability periods were then identified by the main periodogram peaks with confidence levels greater than 99% (De Medeiros et al. 2013).

2.4. The Wavelet Analysis

The wavelet transform (e.g., Grossmann & Morlet 1984) is a powerful tool to analyze a time series in the time-frequency domain, namely by decomposing periodicities as power spectra sections along the time window of the data. This method is comparable to the short-term Fourier transform (STFT)

(Gabor 1946), which decomposes a time series into Fourier transforms of short-term boxes along the time window. The boxes in the STFT, however, have fixed lengths that may typically hinder lower-frequency signals if a high temporal resolution is aimed. The wavelet transform overcomes such a resolution issue by convolving the time series with an orthonormal function called *mother wavelet* with variable dilation and translation parameters that self-adjust to the different frequencies of a signal. The time-frequency diagram of a wavelet transform, namely the wavelet map or local wavelet spectrum, thus decomposes a signal into all frequencies naturally, within a region of confidence, without the need of defining some box length. In addition, a global power spectrum can also be obtained by integrating the wavelet map along the time axis. This global wavelet spectrum gives us a view of the main periodicities present in a time series that can be compared with other power spectra, such as those from FFT and Lomb-Scargle. Overall, the wavelet technique is a useful tool for analyzing non-stationary and non-periodic signals, revealing characteristics that can vary in both time and frequency (Burrus, Gopinath & Guo 1998). To date, a plethora of problems in Astronomy, mostly associated to the search for periodicities have been treated on the basis of the wavelet technique (e.g.: Espaillat et al. 2008; Bravo et al. 2014; Mathur et al. 2014; Bewketu-Belete, A. et al. 2018; de Lira et al. 2019; Santos et al. 2019; Reinhold & Hekker 2020).

The wavelet maps can reveal detailed signatures of a variability behavior that may not be evident in the time series itself or in global power spectra. Therefore, the wavelet method helps us very much in the identification of the types of variability identified in a LC. We refer to Bravo et al. (2014) for a detailed analysis of different signatures that can be observed in wavelet maps of stellar LCs. An important example is the case of analyzing double-dip rotational modulations (Basri & Nguyen 2018) to obtain proper rotation periods rather than aliases. The typical signature of such a case observed in the wavelet map is the presence of two dominant features along time, the period of a feature being the double or a half of the other. In many cases, the rotation period tends to be the longer-period feature, the shorter-period one being an effect of the superposition of two semi-sinusoids associated to the double-dip signature. Figure 5 from Bravo et al. (2014) illustrates a typical example of such a

case. Nevertheless, careful inspection of the LCs along with different tools is necessary for a proper conclusion of the actual period.

2.5. Visual inspection

Once the FFT, Lomb-Scargle and wavelet results in hands, we perform a visual inspection on each LC to identify effective modulation traces based on the procedure applied by De Medeiros et al. (2013). Readers are referred to Sect. 2.1 for a short description of the signatures searched in this work and to Sect. 2.2.2 of De Medeiros et al. (2013) for a detailed discussion on such procedure. Following those authors, we considered that stars with more than three observed cycles in their LCs have confident periods, where the effective number of cycles (N_{Cycle}) is the effective time span (t_{SPAN}) of the LC, excluding gaps, divided by the rotation period (P_{rot}). Nevertheless, stars with $2.5 \leq N_{Cycle} < 3.0$ whose LCs show clear rotation signature with large-amplitude fluctuation, persistent all along the effective time span, were also considered to have confident periods. Figure 1 displays examples of LCs presenting typical rotation signature identified in our sample, with the corresponding FFT and Lomb-Scargle periodograms, as well as the wavelet maps. Figures following the same design of Fig. 1 are provided in the online material for all the stars with rotation and other variability signatures revealed by our analysis.

3. RESULTS

We have analyzed a total of 1000 targets presenting public LCs, with short-cadence TESS observations in sectors 1 to 22, classified as TESS Objects of Interest. Among those stars, we have identified 163 targets with rotation signature, including 131 with unambiguous rotation periodicities, 32 targets with rotation signature but having dubious values for the periods, and 109 stars with ambiguous variability. Dubious rotation periods correspond to stars showing potential rotation signature, but whose period could not be disentangled among two or more possibilities (from periodogram peaks and wavelet maps), as well as stars with $N_{Cycle} < 3$, except for some cases with $2.5 < N_{Cycle} < 3$ that show clear and persistent rotation pattern along their LCs (see Sect. 2.5). Ambiguous variability corresponds to stars showing visually noticeable fluctuations that are faint for proper interpretation

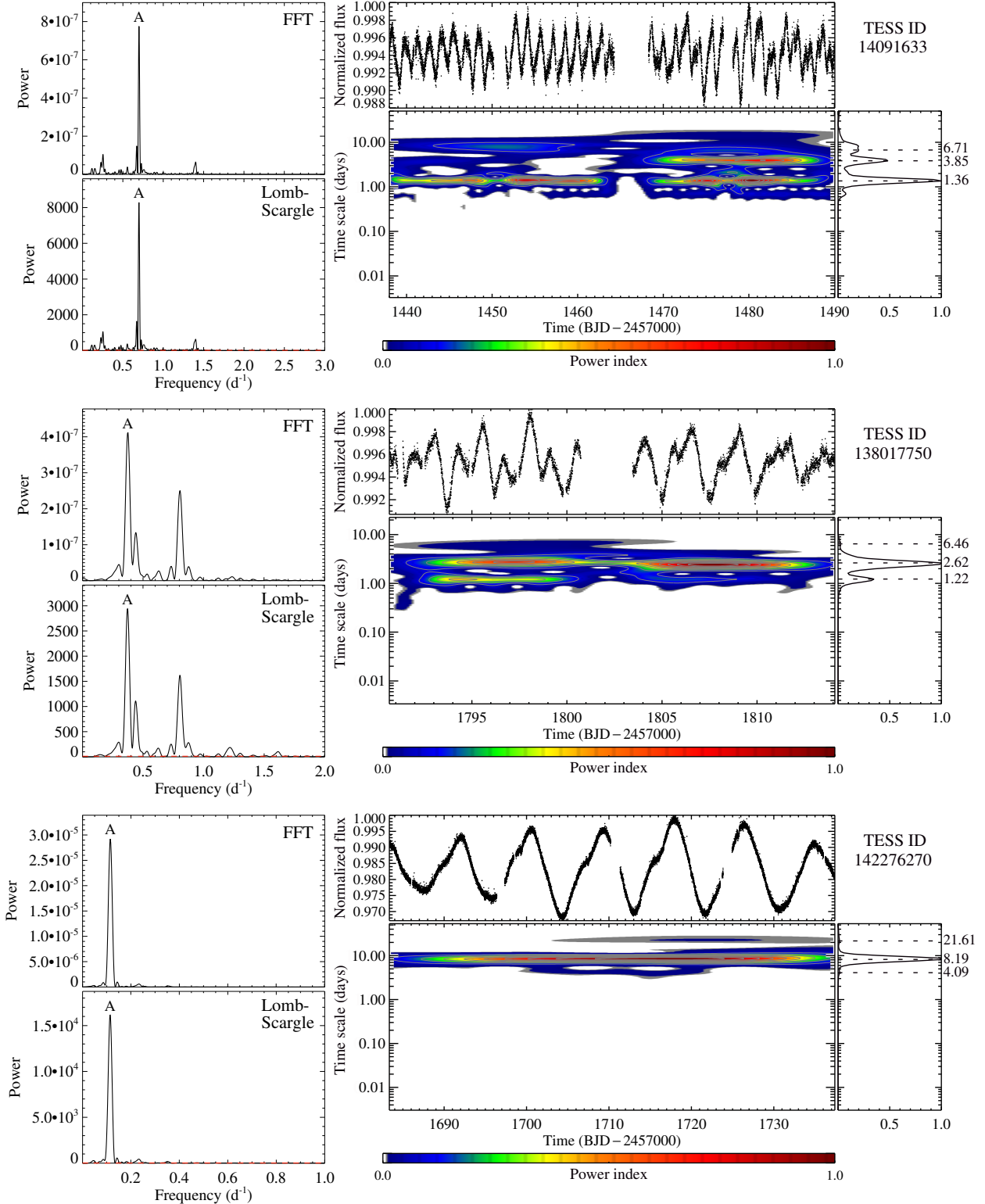


Figure 1. Examples of diagnostic plots displaying FFT and Lomb-Scargle periodograms, LCs and wavelet maps for three TOIs with typical rotation signatures. Persistent periods of 1.361, 2.623, and 8.189 days, respectively, for TIC 14091633 (top panels), TIC 138017750 (middle panels), and TIC 142276270 (bottom panels), are observed in their wavelet maps and confirmed by FFT and Lomb-Scargle peaks labeled *A*. The complete figure set (131 images) is available in the online journal.

or with insufficient time span for proper signature identification, as well as significant large-amplitude variations with a very irregular or complex behavior usually caused by systematics. Some clear variabilities may eventually be classified as ambiguous when could not be discriminated among rotation, pulsation or other signature, as described in Sect. 2.1, and those cases shall be revisited in future works, especially using additional observations. Figure 2 displays typical examples of LCs with dubious rotation periods and ambiguous variability. Table 1 lists stars with unambiguous rotation periodicities. For each star, from left to right, the columns show the following: the TIC ID, stellar coordinates, stellar parameters (T_{eff} and $\log g$), orbital period (P_{orb}), rotation period (P_{rot}), error in the rotation period (eP_{rot}), effective time span (t_{SPAN}) of each LC (the total time span subtracted by the duration of eventual gaps), the effective number of cycles of the rotational modulation (defined as $N_{Cycle} = t_{SPAN}/P_{rot}$), and the TESS observation sectors. Table 2 lists the TOIs with dubious rotation periods, whereas Table 3 lists the stars with ambiguous variability.

The fraction of stars that show rotational modulation is 16% of the parent sample of 1000 TOIs considered in this work. Indeed, the detection of stellar variability it depends strongly on instrumental characteristics, such as photometric sensitivity, time span of the observation (see, e.g., Leão et al. 2015), and even on LCs reduction and treatment procedures used (de Lira et al. 2019). For instance, rotational modulation was detected for no more than 5% of the total sample of CoRoT stars (e.g., Meibom et al. 2011; De Medeiros et al. 2013), whereas for the total sample of *Kepler* stars that fraction increased to about 20% (e.g., Nielsen et al. 2013; McQuillan et al. 2013a,b, 2014; Reinhold et al. 2013; Walkowicz & Basri 2013; Paz-Chinchón et al. 2015; Reinhold & Hekker 2020). The rotation signature detected in 16% of the stars in our sample is in agreement with that found in *Kepler* stars. Among those targets with unambiguous rotation, the following targets exhibit potential flare events with the date of the major feature indicated: TIC 200322593 (Nov 25, 2018), TIC 233211762 (Nov 9, 2019), TIC 244161191 (Oct 3, 2018), TIC 257605131 (Oct 20, 2018), TIC 278198753 (May 27, 2019), TIC 300293197 (Nov 21, 2018), TIC 307610438 (May 1, 2019), TIC 318937509 (Jan 16, 2019), TIC 32830028 (Dec 23, 2018), TIC 348538431 (Jan 28, 2019), TIC 460205581 (May 3, 2019), TIC 47384844 (Mar 11, 2019), TIC 67646988 (Feb 12, 2020), TIC 77951245 (Nov 19, 2018), TIC 93125144

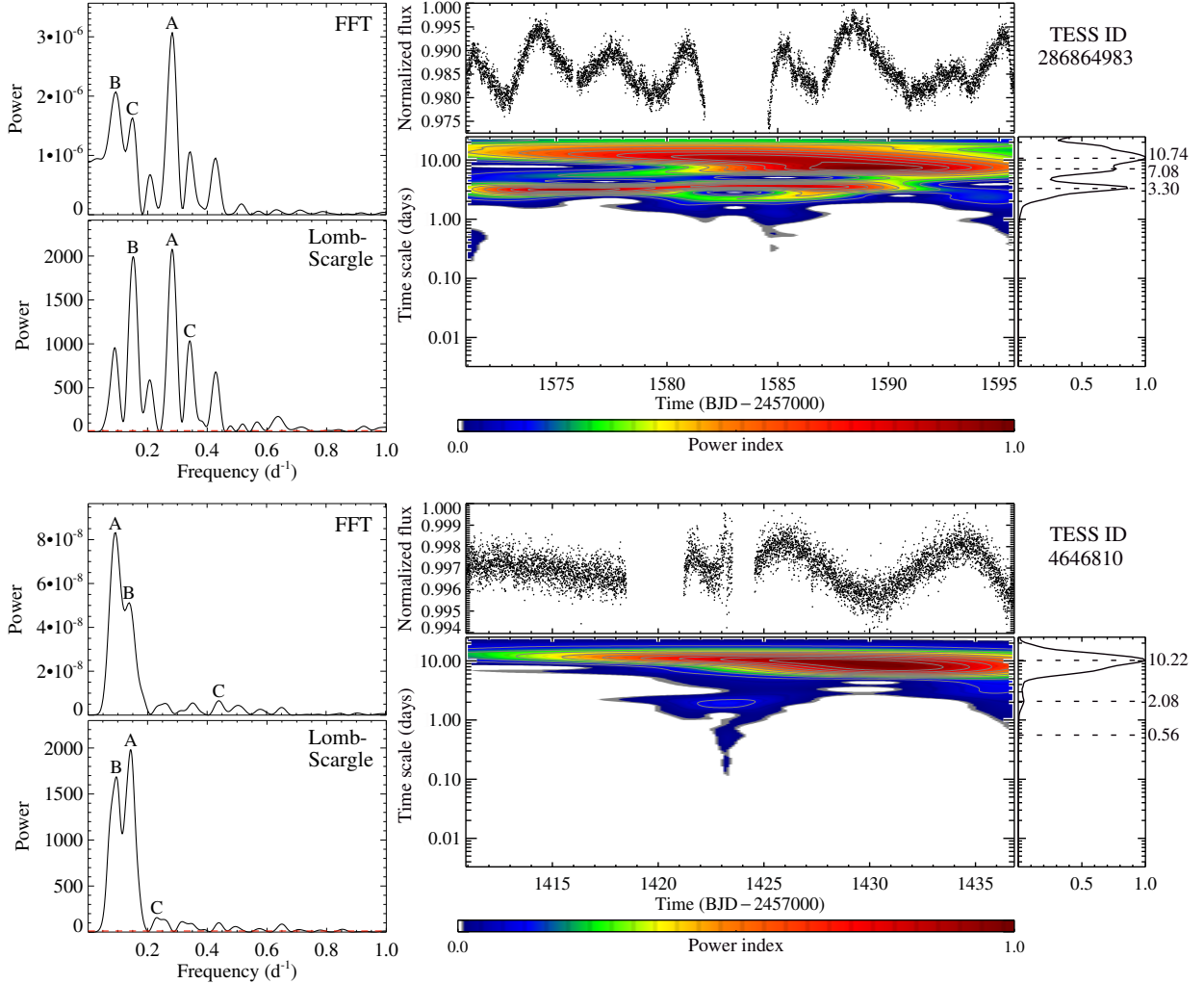


Figure 2. Examples of diagnostic plots displaying FFT and Lomb-Scargle periodograms, LCs and wavelet maps for two TOIs showing typical characteristics of dubious rotation periods (top panels, TIC 286864983) and ambiguous variability (bottom panels, TIC 4646810). In the top panels, in spite of a potential rotation signature, periodograms and wavelet map reveal a multiple periodicity of no clear diagnosis. In the bottom panels, the LC seems irregular with no apparent variability at the beginning, some systematics in the middle, and a possible variability at the second half.

(Dec 22, 2018), and TIC 98796344 (Nov 7, 2018). Five other stars with unambiguous rotation, TIC 70797900, TIC 235037761, TIC 299798795, TIC 206609630, and TIC 410214986 also exhibit flare events as previously reported by Günther et al. (2020). In addition, one star with dubious rotation period, TIC 233120979, and two stars with ambiguous variability, TIC 13684720 and TIC 89256802,

Table 1. Catalog of TOIs with unambiguous rotation periods from our analysis.

TIC ID	T_{eff}	$\log g$	P_{orb}	P_{rot}	eP_{rot}	t_{SPAN}	N_{Cycle}	Sectors
	(K)	(dex)	(days)	(days)	(days)	(days)		
2760710	2808	5.206		1.251	0.033	24	19.2	2
7624182	8666	3.801	1.108	1.624	0.029	45	27.7	4
9033144	5757	3.900	4.715	4.201	0.368	24	5.7	2
9348006	5251	4.543	10.240	5.329	0.592	24	4.5	21
13499636	5518	4.592	11.325	5.595	0.921	17	3.0	15
14091633	6350	4.340	5.529	1.363	0.022	43	31.5	5
...

NOTE—With one row for each TOI, the following information is listed: the TIC ID, effective temperature (T_{eff}), surface gravity ($\log g$), and orbital period (P_{orb}) taken from the TOI Release Portal (<https://tess.mit.edu/toi-releases/>), rotation period (P_{rot}), error in the rotation period (eP_{rot}), effective time span (t_{SPAN}), and effective number of cycles (N_{Cycle}), obtained from our analysis, and TESS observation sectors. Values for $\log g$ and P_{orb} are rounded to 3 decimal digits. The complete table is provided in machine-readable form in the online journal. Here we show a fragment for guidance regarding its form and content.

show flare events with the major one at September 9th 2019, August 2nd 2019, and November 10th 2018, respectively. Günther et al. (2020) also reported flare events for TIC 32090583.

It is worthy to underline the large number of 714 TOIs exhibiting a noisy behavior in their LCs, corresponding to 71% of the parent sample. Although those stars present typically low-amplitude signals whose physical periodicities cannot be easily identified, from a certain view they can also point for key information. Typically, a noisy signature is a complex combination of instrumental noise contributions (related, for instance, with Poisson statistics and readout noise) plus a relevant contribution of intrinsic stellar noise, Galactic position, light from neighboring stars and sky back-

Table 2. List of the 32 TOIs with dubious rotation periods from our analysis.

TIC ID	T_{eff}	$\log g$	P_{orb}	P_{rot}	t_{SPAN}	N_{Cycle}	Sectors
	(K)	(dex)	(days)	(days)	(days)	(days)	
1129033	5500	4.483	1.360	5.00/10.00	19	1.9	4
1528696	4975	4.520	0.882	5.15/8.97	23	2.6	5
9006668	5024	4.569	1.272	7.05/9.96	25	2.5	2
35516889	5568	4.393	0.789	6.18/9.37	19	2.0	9
36734222	4400	4.646	0.813	7.40 ^a	19	2.6	9
62483237	4356	4.535	11.058	6.83/11.09	24	2.2	1
...

NOTE—The following information is listed: the TIC ID, effective temperature (T_{eff}), surface gravity ($\log g$), and orbital period (P_{orb}) taken from the TOI Release Portal (<https://tess.mit.edu/toi-releases/>), likely rotation period values (P_{rot}), effective time span (t_{SPAN}), and effective number of cycles (N_{Cycle}), obtained from our analysis, and TESS observation sectors. Flag *a* corresponds to stars with less than three observed cycles that show non-persistent pattern along their LCs. Values for $\log g$ and P_{orb} are rounded to 3 decimal digits. The complete table is provided in machine-readable form in the online journal. Here we show a fragment for guidance regarding its form and content.

ground contamination (e.g.: Gilliland et al. 2011). When the TOI LCs considered in this work present a low-amplitude signal, we assume them to be a noisy signature. Nevertheless, for some stars the noisy behavior could reflect low activity or long periodicities, in particular for those targets with short observational time span. It should be noticed that part of the stars classified as having noisy LCs may have been set up this way because of data reduction issues. As such, caution should be taken with this subsample when using it for planet search strategies. Additional observations and data treatments may change the status of some of these stars. Table 4 lists the stars with noisy LCs.

Table 3. List of the 109 TOIs with ambiguous variability behavior from our analysis.

TIC ID	T_{eff}	$\log g$	P_{orb}	t_{SPAN}	Sectors
	(K)	(dex)	(days)	(days)	
1003831	5752	4.471	1.651	18	8
1103432	6231	4.264	3.728	17	8
4646810	4884	4.490	14.490	21	4
9804616	3274	4.979	0.517	19	4
12862099	5410	4.479	2.424	17	3
13684720	3275	4.758	12.438	36	14,15
...

NOTE—The following information is listed: the TIC ID, effective temperature (T_{eff}), surface gravity ($\log g$), and orbital period (P_{orb}) taken from the TOI Release Portal (<https://tess.mit.edu/toi-releases/>), effective time span (t_{SPAN}) obtained from our analysis, and TESS observation sectors. Values for $\log g$ and P_{orb} are rounded to 3 decimals digits. The complete table is provided in machine-readable form in the online journal. Here we show a fragment for guidance regarding its form and content.

Among those targets with noisy LCs, six of them, TIC 186812530, TIC 230086768, TIC 286865921, TIC 365639282, and TIC 36622912 exhibit potential flare events, with major features at January 28th 2019, September 2nd 2019, April 17th 2019, December 16th 2018, and January 16th 2019, respectively. The noisy-LC star TIC 272086159 also exhibits flare events as reported by Günther et al. (2020).

Table 4. List of the 714 TOIs with noisy LCs from our analysis.

TIC ID	T_{eff}	$\log g$	P_{orb}	t_{SPAN}	Sectors
	(K)	(dex)	(days)	(days)	
1133072	3380	4.925	0.847	15	8
1449640	6383	4.030	3.502	23	5
4616072	6675	4.201	4.186	40	6
4897275	5854	4.386	16.710	24	21
5868998	3602	4.817	0.636	18	10
6663331	5498	4.479	3.180	23	13
...

NOTE—The following information is listed: the TIC ID, effective temperature (T_{eff}), surface gravity ($\log g$), and orbital period (P_{orb}) taken from the TOI Release Portal (<https://tess.mit.edu/toi-releases/>), effective time span (t_{SPAN}) obtained from our analysis, and TESS observation sectors. Values for $\log g$ and P_{orb} are rounded to 3 decimal digits. The complete table is provided in machine-readable form in the online journal. Here we show a fragment for guidance regarding its form and content.

Based on the rotation periods and other stellar parameters listed in Tabs. 1 to 4, the following major scenarios emerge. First, the whole sample of 1000 TOIs covers a range of effective temperature from 2,808 K to 9,898 K, typically stars of spectral type from M6 to A0, a scenario followed by the stars with rotation signature, ambiguous variability and noisy LCs. Figure 3 illustrates the effective temperature distributions for the underlined samples. Second, the distribution of the different subsample of stars, namely stars with rotation signature (with unambiguous and dubious periodicities), stars showing

ambiguous stellar variability, and stars with noisy behavior, follow, approximately, the same trend in the $\log g$ versus T_{eff} diagram as displayed in Fig. 4. Third, as it arises in Fig. 5, the distribution of the rotational periods ranges between 0.321 and 13.219 days. Overall, the range of this distribution is associated to the TESS technical limits of 28 days baseline per sector, which does not favor the determination of longer periods of rotation, also common among M dwarf stars (e.g.: Newton et al. 2018; Oelkers et al. 2018), but only periods shorter than 28 days. Even for the LCs obtained from combined sectors, thus with long time spans, the post-treatments needed in this process may hinder longer periodicities. The rotation period distribution also reveals a trend for a bimodality, with a peak around 5 days and a second one arising around 8 days. Such a trend reflects what is expected for cool stars, as reported by McQuillan (2013, 2014) and Davenport (2017). However, caution should be taken in its interpretation, which could be associated to the present sample limitation, especially at lower temperatures.

As a by-product of our analysis, the present study has also revealed 10 TOIs with pulsation signatures, with periodicities ranging from 0.049 to 2.995 days. Figure 6 displays three examples of these pulsating TOIs. A more detailed study would be needed to confirm specific classes of pulsators, a subject that is beyond the scope of the present paper. Table 5 lists these stars with the respective pulsating periods. We have also identified four eclipsing binaries, TIC 9727392, TIC 100100827, TIC 149010208, and TIC 432549364, with orbital periods of 4.534, 0.942, 3.437, and 1.217 days, respectively; the star TIC 149010208 also exhibits two clear flares at September 3rd and 18th 2018.

3.1. *KELT periodicities for TOI stars*

The Kilodegree Extremely Little Telescope (KELT) project (Pepper et al. 2007; 2012), has been surveying bright stars with a typical cadence between 10–30 minutes, for more than four million sources with apparent visual magnitudes in the approximate range $7 < V < 13$. Dedicated to the search of transiting of large-radii planets, KELT has also supported studies on the variability of thousands of stars. Oelkers et al. (2018) provided a catalog of 62,229 stars presenting significant large-amplitude fluctuations probably caused by stellar rotation. Indeed, this survey provides rotation periods for a significant amount of stars in common with the TESS catalog, using a homogeneous

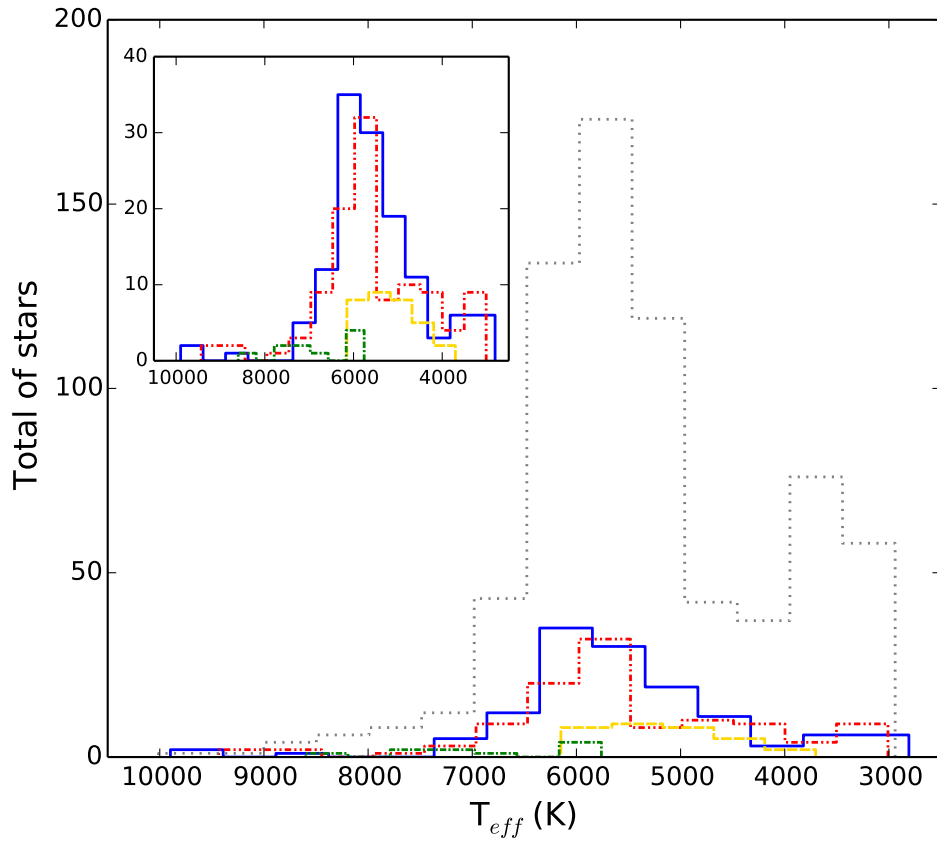


Figure 3. The distribution of the effective temperature for the TOIs analyzed in the present study. Lines in solid blue, dashed orange, dot-dashed green, and dot-dot-dashed red, and dashed gray are for stars with unambiguous rotation periods, dubious rotation periods, pulsation, and ambiguous variability, and noisy LCs, respectively. A closer view of the distribution of the effective temperature without the subsample of stars with noisy LCs is displayed in the upper left corner of the figure for better visualization.

procedure, offering the possibility of a comparison with periods obtained from the present study. Fourty objects of our present sample of TOIs are listed by those authors as stars with likely rotation periods.

For seventeen of the referred stars we have identified only noise in their TESS LCs, whereas the eighteen additional stars have confirmed rotation periods. As shown in Table 6, for this second group, the rotation periods for 9 stars are in agreement, within a range of 10%, and the other 9 stars are in disagreement, when comparing our period measurements with those by Oelkers et al. (2018). Table

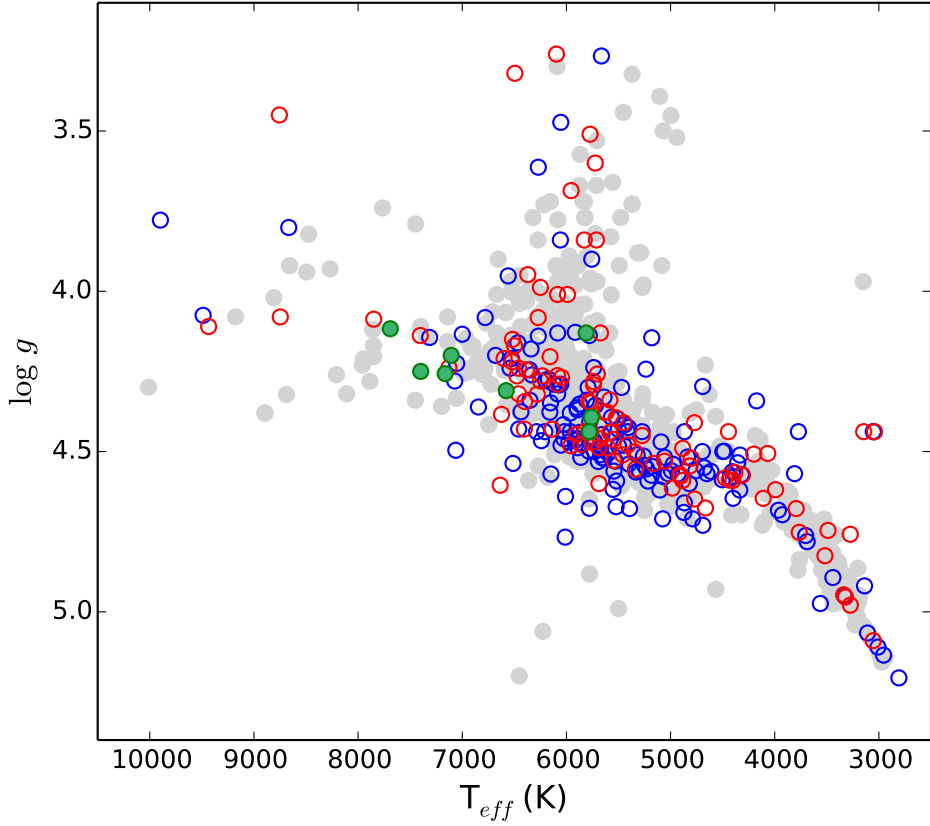


Figure 4. The T_{eff} versus $\log g$ diagram for the sample of 1000 TOIs composing the present study. Circles in open blue, solid green, open red, and solid gray are for stars with unambiguous and dubious rotation periods, pulsation, ambiguous variability, and noisy LCs, respectively. The distributions of TOIs with rotation, ambiguous variability, and noisy LCs follow fairly the same scenario.

7 lists the sub-sample of TOI stars with noisy LCs, with the periodicities computed by Oelkers et al. (2018) ranging from about 0.9 to 47 days. A comparison between rotation periods measured in the present study and those estimated by Oelkers et al. (2018) should be taken with cautious because different aspects are involved in the observational procedures, including the cadence of observations, observational time spans and, in particular, the photometric precisions. Nevertheless, it is worthy to underline that for the noisy stars from TESS, namely those stars for which we have found no periodicities, Oelkers et al. (2018) were able to estimate periods for 12 stars with values larger than

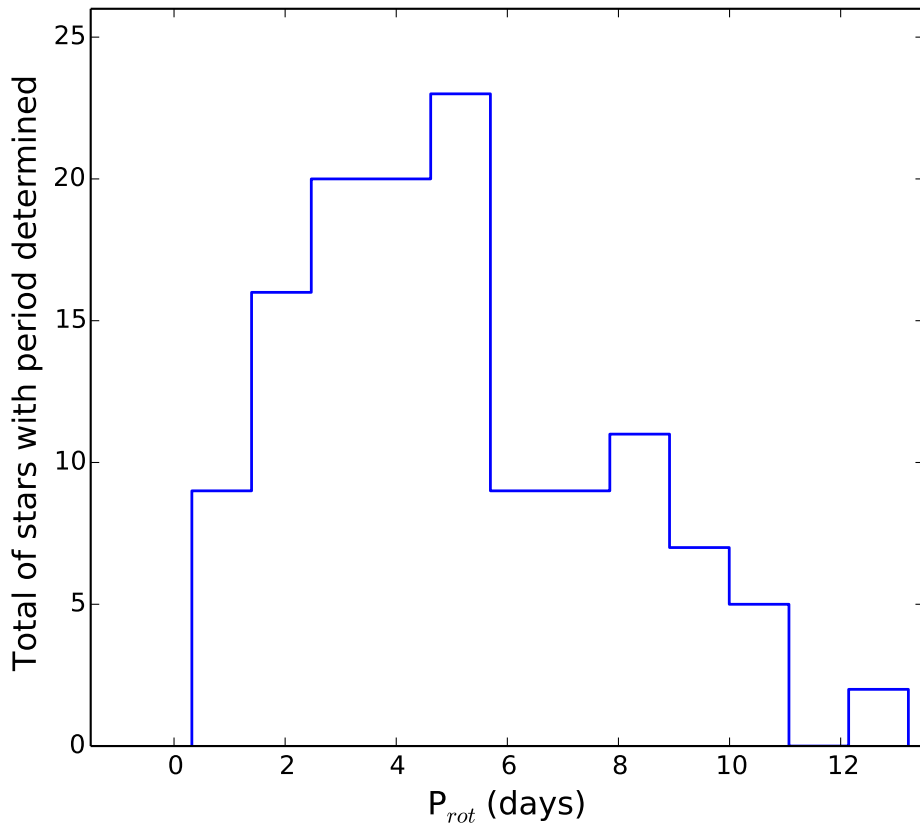


Figure 5. The rotation period distribution for the 131 TOI stars exhibiting unambiguous rotation signatures from the present analysis.

14 days. For these noisy stars low activity or long rotation periods are expected, which is fairly in parallel with the high periods found by Oelkers et al. (2018).

4. SUMMARY

We conduct an in-depth search for rotation and pulsation signatures from a sample of 1000 TOI stars observed in 2-min cadence by TESS. Such an analysis was based on three procedures, namely wavelet, Fast Fourier Transform and Lomb-Scargle, along with a meticulous visual inspection. We identified 163 TOIs with clear rotational modulation, from which 131 stars present unambiguous rotation period, ranging from 0.321 to 13.219 days, one of these stars being fast rotator with $P_{rot} < 0.50$ days, and 32 of them presenting dubious values for the periodicity. The present analysis revealed also four eclipsing binaries, ten stars presenting clear signatures of pulsation, with periods ranging

Table 5. TOI stars with unambiguous pulsation periodicity from our analysis.

TIC ID	T_{eff} (K)	$\log g$ (dex)	P_{orb} (days)	P_{pul} (days)	eP_{pul} (days)	t_{SPAN} (days)	N_{Cycle}	Sectors
129979528	7399	4.250	1.220	0.049	0.001	17	346.9	18
149833117	6578	4.310	4.052	0.303	0.002	23	75.4	20
156987351	7691	4.117	3.063	0.082	0.001	39	475.6	6
164173105	7164	4.257	3.073	0.572	0.008	20	35.9	16
201604954	5760	4.393	4.606	0.629	0.008	25	40.1	13
287196418	7106	4.200	3.695	1.016	0.009	61	60.2	14,16,17
297967252	8599		9.683	1.128	0.014	45	39.5	9
329277372	5780	4.438	2.888	0.524	0.003	40	77.4	16
350132371	5811	4.130	1.032	1.990	0.035	56	28.2	16,17,18
374095457	5780	4.438	0.784	2.995	0.125	36	11.9	10 9

NOTE—The following information is listed: the TIC ID, effective temperature (T_{eff}), surface gravity ($\log g$), and orbital period (P_{orb}) taken from the TOI Release Portal (<https://tess.mit.edu/toi-releases/>), pulsation period (P_{pul}), error in the pulsation period (eP_{pul}), effective time span (t_{SPAN}), and effective number of cycles (N_{Cycle}), obtained from our analysis, and TESS observation sectors. Values for $\log g$ and P_{orb} are rounded to 3 decimals digits.

from 0.049 to 2.995 days, and 109 stars show ambiguous variability, whose astrophysical root-cause is not clearly identified. For the remaining 714 TOIs the TESS light curves show essentially a noisy pattern, with low amplitude signals. Whereas the signatures of rotation reflect the presence of prominent star spots at different locations in the stellar surface, the stars with ambiguous variability and noisy pattern appear to reflect a large number of causes, including polar spots, low activity phases and long periodicity. In this sense, among the 17 stars with TESS LCs presenting noisy pattern, in common with KELT observations, 12 have KELT periods ranging from 14 to 47 days, therefore rotating slower than our sample with unambiguous rotation periodicities. The scenario for rotation from an analysis combining the present results with those from Oelkers et al. (2018) tend

Table 6. TOI stars with unambiguous rotation from our analysis in common with the KELT catalog of rotation periodicity (Oelkers et al. 2018).

TIC ID	P _{rot}	P _{rot}
	Our work (days)	KELT (days)
9348006	5.329	15.7332
13499636	5.595	1.12709
22843856	3.518	3.8088
29191596	9.070	9.88338
138017750	2.623	1.23605
153949511	8.095	27.1518
156991337	3.607	3.76619
201248411	13.219	12.7535
207141131	8.490	8.69263
219776325	9.330	10.0806
220459826	5.559	0.521154
229938290	8.600	1.30302
235037761	7.359	7.30887
241196395	2.019	1.04978
293954617	5.368	11.7178
356311210	5.356	5.36711
382474101	2.722	0.728157
459970307	3.581	7.05368

Table 7. TOI stars with a noisy behavior from our analysis in common with the KELT catalog of rotation periodicity (Oelkers et al. 2018).

TIC ID	P_{rot} (KELT) (days)
69679391	29.5334
115771549	35.8166
130924120	14.1864
134200185	45.4959
167754523	17.6585
207084429	14.1864
237928815	21.3995
257241363	32.3729
279741379	47.6417
286355915	0.961816
306996324	1.04328
309792357	1.04328
322063810	0.902519
377293776	25.1256
403224672	1.12583
406672232	30.4229
413248763	20.5297

to follow fairly the same trend observed by different authors (e.g.: Leão et al. 2015; Paz-Chinchón et al. 2015; McQuillan et al. 2013), in particular for *Kepler* stars with planet candidates. As reported by those authors, rotation period for M to F stars are distributed typically from about 1 to 80 days.

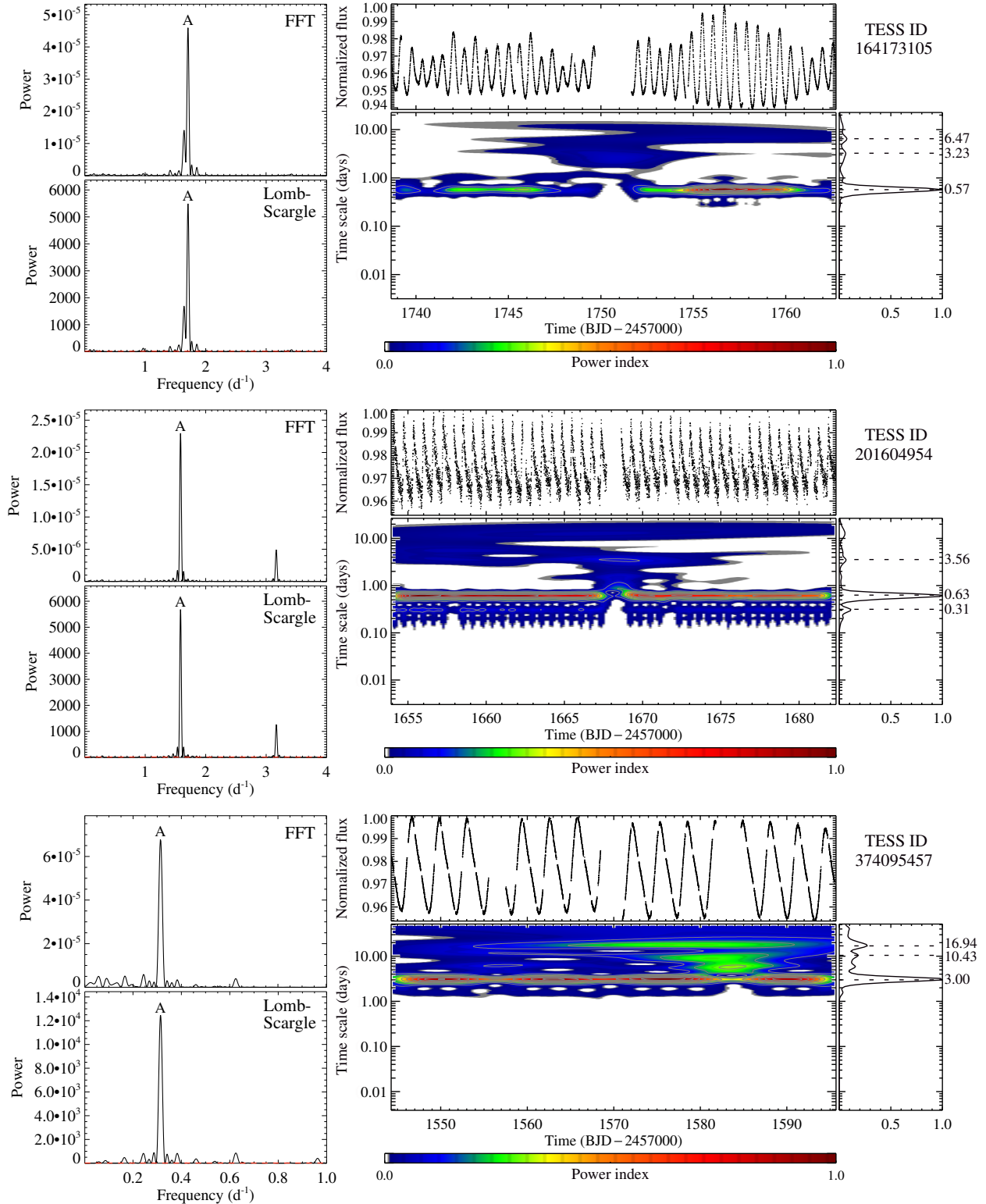


Figure 6. Examples of diagnostic plots displaying FFT and Lomb-Scargle periodograms, LCs and wavelet maps for three TOIs with typical pulsation signatures. Persistent periods of 0.572, 0.629, and 2.995 days, respectively, for TIC 164173105 (top panels), TIC 201604954 (middle panels), and TIC 374095457 (bottom panels), are observed in their wavelet maps and confirmed by FFT and Lomb-Scargle peaks labeled *A*.

In addition, studies measuring the rotation periods of nearby low-mass stars (Newton et al. 2016, 2018) have identified a population of fast rotators ($P_{rot} < 10$ d) and a population of slow rotators ($P_{rot} > 70$ d), a fact that is followed by the present results considering only the group of fast rotators found by those authors.

We shall also touch upon some particularities emerging from the present analysis: 22 stars have $P_{rot} \simeq P_{orb}$. Within the observational uncertainties, this finding points for potential targets undergoing a stage of tidal synchronization. This study revealed also 23 TOIs with unambiguous rotation period showing two periods, one being approximately the double or a half of the rotation period, as it can be clearly seen in the wavelet maps (e.g., Fig. 1, middle panel). As mentioned in Sects. 2.1 and 2.4 and as described in Basri & Nguyen (2018), this is a common pattern observed in rotating stars that is overall related to hemispherical asymmetries. Although those asymmetries may be associated to a complex spot distribution and dynamics, they can be explored with the help of relatively simple spot modeling, providing thus important clues for the study of spot dynamics and differential rotation (e.g.: Lanza et al. 2014; Aigrain et al. 2015; das Chagas et al. 2016). Another particular aspect regards to the group of ten stars with pulsation, which offers additional perspectives to explore the frequency modulation methods (Shibahashi & Kurtz 2012), to derive information traditionally obtained from radial velocity procedure (e.g.: Murphy et al. 2014, 2016; Hermes 2018).

Let us also underline that all the types of stellar variability, as source of identified astrophysical phenomena or noise, can impact directly on the precision and accuracy of exoplanet multi-band photometric transit and spectroscopic observations. Fast rotators, particularly, can inhibit the detection of small planets (e.g.: Berta et al. 2012; Kipping et al. 2017), whereas measurements of planetary mass can be hindered if a star and its planet are in tidal synchronization. In this sense, the results pointed out in this paper offer also constraints to predict the impact of stellar variability resulting from rotation and pulsation on observations dedicated to the characterization of planets around TOI stars, and present a methodology that could be applied to other samples of stars with or without planetary companions. As TESS continues to observe the sky, it will produce a large quantity of

2-min cadence LCs for thousands of stars, an additional unique laboratory for the continuation of the work reported here.

Finally, this study reinforces an important lesson: for identifying periodicities with real physical meaning, it is not sufficient the selection of numbers emerged from periodograms obtained from a single computational method. In many occasions, such periods may be mere artifacts of the method used or may represent only estimations. In this context, obtaining periodicities based on multiple methods that combine information from different types of periodograms together with wavelet analysis, which provides the identification of periodicity associated with the persistence of the phenomenon, as well as with a visual inspection of the LC, is the recommended path for a more confident determination of periodicities with clear astrophysical meaning.

The full catalog has been uploaded at the Filtergraph portal⁶ (Burger et al. 2013) for data visualization. The portal can be used to access the variability and periodicity information described in this study: stellar parameters obtained from the TESS data basis, LC, FFT and Lomb-Scargle periodograms, and wavelet maps for each TOI star. This portal is meant to be a living database and will be updated with new rotation and pulsation periods as soon as new TOIs LCs become public at the TESS portal.

⁶ https://filtergraph.com/tess_rotation_tois

ACKNOWLEDGMENTS

We warmly thank our families for involving us with care, patience, and tenderness, during the home office tasks for the preparation of this work face to this COVID-19 difficult moment. Research activities of the observational astronomy board at the Federal University of Rio Grande do Norte are supported by continuous grants from the brazilian funding agencies CNPq, FAPERJ, and INCT-INESPAO. This study was financed in part by the Coordenação de Aperfeiçoamento de Pessoal de Nível Superior - Brasil (CAPES) - Finance Code 001. RLG, YSM, and MAT acknowledge CAPES graduate fellowships, and ABB acknowledges CNPq graduate fellowship. JPB acknowledges a CAPES/PNPD fellowship. ICL, BLCM, and JRM acknowledge CNPq research fellowships. This paper includes data collected by the TESS mission. Funding for the TESS mission is provided by the NASA Explorer Program. The research described in this paper makes use of Filtergraph, an online data visualization tool developed at Vanderbilt University through the Vanderbilt Initiative in Data-intensive Astrophysics (VIDA) and the Frist Center for Autism and Innovation (FCAI). We warmly thank the Referee for comments and suggestions that clarified important aspects of this study.

REFERENCES

- Aigrain, S., Llama, J., Ceillier, T., et al. 2015, MNRAS, 450, 3211
- Baglin, A., Auvergne, M., Barge, P., et al. 2009, in IAU Symposium, Vol. 253, Transiting Planets, ed. F. Pont, D. Sasselov, & M. J. Holman, 7181
- Bányai, E., Kiss, L. L., Bedding, T. R., et al. 2013, MNRAS, 436, 1576
- Basri, G., Walkowicz, L. M., Batalha, N., et al. 2011, AJ, 141, 20
- Basri, G. 2018, ApJ, 865, 142
- Basri, G., & Nguyen, H. T. 2018, ApJ, 863, 190
- Berta, Z. K., Irwin, J., Charbonneau, D., et al. 2012, AJ, 144, 145
- Bewketu Belete, A., Femmam, S., Tornikoski, M., et al. 2019, ApJ, 873, 108
- Borucki, W. J., Koch, D., Basri, G., et al. 2010, Science, 327, 977
- Bravo, J. P., Roque, S., Estrela, R., et al. 2014, A&A, 568, A34
- Burger, D., Stassun, K. G., Pepper, J., et al. 2013, Astronomy and Computing, 2, 40
- Canto Martins, B. L., Das Chagas, M. L., Alves, S., et al. 2011, A&A, 530, A73
- Cooley, J. W., & Tukey, J. W. 1965 Math. Comp. 19, 297

- Costa, A. D., Canto Martins, B. L., Bravo, J. P., et al. 2015, ApJL, 807, L21
- Cunha, M. S., Antoci, V., Holdsworth, D. L., et al. 2019, MNRAS, 487, 3523
- Das Chagas, M. L., Bravo, J. P., Costa, A. D., et al. 2016, MNRAS, 463, 1624
- Davenport, J. R. A. 2017, ApJ, 835, 16
- de Freitas, D. B., Leão, I. C., Ferreira Lopes, C. E., et al. 2013, ApJL, 773, L18
- de Lira, S. R., Bravo, J. P., Leão, I. C., et al. 2019, MNRAS, 484, 3935
- De Medeiros, J. R., Ferreira Lopes, C. E., Leão, I. C., et al. 2013, A&A, 555, A63
- Donnelly, R. F., & Puga, L. C. 1990, SoPh, 130, 369
- Doyle, L., Ramsay, G., & Doyle, J. G. 2020, MNRAS, doi:10.1093/mnras/staa923
- Espaillat, C., Bregman, J., Hughes, P., et al. 2008, ApJ, 679, 182
- Ferreira Lopes, C. E., Neves, V., Leão, I. C., et al. 2015, A&A, 583, A122
- Gabor, D. 1946, J. Inst. Electr. Eng., 93, 429
- Gilliland, R. L., Chaplin, W. J., Dunham, E. W., et al. 2011, ApJS, 197, 6
- Grossmann, A., & Morlet, J. 1984, SIAM J. Math. Anal. 15, 723
- Günther M. N., 2019, ESS, 51, 331.06
- Günther, M. N., Zhan, Z., Seager, S., et al. 2020, AJ, 159, 60
- Hermes J. J., 2018, haex.book, 6
- Horne, J. H., & Baliunas, S. L. 1986, ApJ, 302, 757
- Irwin, J., & Bouvier, J. 2009, IAUS, 258, 363
- Jenkins, J. M., Twicken, J. D., McCauliff, S., et al. 2016, Proc. SPIE, 99133E
- Kawaler S. D., 2015, ASPC, 493, 65
- Kipping, D. M., Cameron, C., Hartman, J. D., et al. 2017, AJ, 153, 93
- Lamm, M. H., Bailer-Jones, C. A. L., Mundt, R., et al. 2004, A&A, 417, 557
- Lammer, H., Güdel, M., Kulikov, Y., et al. 2012, EP&S, 64, 179
- Lanza, A. F., Rodonò, M., Pagano, I., et al. 2003, A&A, 403, 1135
- Lanza, A. F., Bonomo, A. S., & Rodonò, M. 2007, A&A, 464, 741
- Lanza, A. F., Pagano, I., Leto, G., et al. 2009, A&A, 493, 193
- Lanza, A. F., Das Chagas, M. L., & De Medeiros, J. R. 2014, A&A, 564, A50
- Leão, I. C., Pasquini, L., Ferreira Lopes, C. E., et al. 2015, A&A, 582, A85
- Lomb, N. R. 1976, Ap&SS, 39, 447
- Lundin, R., Lammer, H., & Ribas, I. 2007, SSRv, 129, 245
- Maoz, D., Mazeh, T., & McQuillan, A. 2015, MNRAS, 447, 1749
- Mathur S., Salabert D., García R. A., Ceillier T., 2014, JSWSC, 4, A15
- McQuillan, A., Aigrain, S., & Mazeh, T. 2013, MNRAS, 432, 1203
- McQuillan, A., Mazeh, T., & Aigrain, S. 2013, ApJL, 775, L11

- McQuillan, A., Mazeh, T., & Aigrain, S. 2014, *ApJS*, 211, 24
- Meibom, S., Barnes, S. A., Latham, D. W., et al. 2011, *ApJL*, 733, L9
- Miller, B. P., Gallo, E., Wright, J. T., et al. 2015, *ApJ*, 799, 163
- Mosser, B., Goupil, M. J., Belkacem, K., et al. 2012, *A&A*, 548, A10
- Murphy, S. J., Bedding, T. R., Shibahashi, H., et al. 2014, *MNRAS*, 441, 2515
- Murphy, S. J., Bedding, T. R., & Shibahashi, H. 2016, *ApJL*, 827, L17
- Nielsen, M. B., Gizon, L., Schunker, H., et al. 2013, *A&A*, 557, L10
- Newton, E. R., Irwin, J., Charbonneau, D., et al. 2016, *ApJ*, 821, 93
- Newton, E. R., Mondrik, N., Irwin, J., et al. 2018, *AJ*, 156, 217
- Oelkers, R. J., Rodriguez, J. E., Stassun, K. G., et al. 2018, *AJ*, 155, 39
- Paz-Chinchón, F., Leão, I. C., Bravo, J. P., et al. 2015, *ApJ*, 803, 69
- Pepper, J., Pogge, R. W., DePoy, D. L., et al. 2007, *PASP*, 119, 923
- Pepper, J., Kuhn, R. B., Siverd, R., et al. 2012, *PASP*, 124, 230
- Press, W. H., & Rybicki, G. B. 1989, *ApJ*, 338, 277
- Reinhold, T., Reiners, A., & Basri, G. 2013, *A&A*, 560, A4
- Reinhold, T., & Hekker, S. 2020, *A&A*, 635, A43
- Ricker, G. R., Winn, J. N., Vanderspek, R., et al. 2015, *JATIS*, 1, 014003
- Sanchis-Ojeda, R., Winn, J. N., Marcy, G. W., et al. 2013, *ApJ*, 775, 54
- Sanchis-Ojeda, R., Rappaport, S., Winn, J. N., et al. 2014, *ApJ*, 787, 47
- Santos, A. R. G., García, R. A., Mathur, S., et al. 2019, *ApJS*, 244, 21
- Scargle, J. D. 1982, *ApJ*, 263, 835
- Shibahashi, H., & Kurtz, D. W. 2012, *MNRAS*, 422, 738
- Smith, J. C., Stumpe, M. C., Van Cleve, J. E., et al. 2012, *PASP*, 124, 1000
- van Saders, J. L., & Pinsonneault, M. H. 2013, *ApJ*, 776, 67
- Viswanath, G., Narang, M., Manoj, P., et al. 2020, *AJ*, 159, 194
- Walkowicz, L. M., Basri, G., & Valenti, J. A. 2013, *ApJS*, 205, 17
- Walkowicz, L. M., & Basri, G. S. 2013, *MNRAS*, 436, 1883
- Zhan, Z., Günther, M. N., Rappaport, S., et al. 2019, *ApJ*, 876, 127

APPENDIX

A. ONLINE MATERIAL

This section brings the entire Tables 1, 2, 3, and 4. Supplementary material supporting this study is also available, including treated light curves, wavelet maps, and periodograms, for stars with unambiguous rotation signatures, dubious rotation periods, and ambiguous variabilities.

Table 1. Catalog of TOIs with unambiguous rotation periods from our analysis.

TIC ID	T_{eff}	$\log g$	P_{orb}	P_{rot}	eP_{rot}	t_{SPAN}	N_{Cycle}	Sectors
	(K)	(dex)	(days)	(days)	(days)	(days)		
2760710	2808	5.206		1.251	0.033	24	19.2	2
7624182	8666	3.801	1.108	1.624	0.029	45	27.7	4
9033144	5757	3.900	4.715	4.201	0.368	24	5.7	2
9348006	5251	4.543	10.240	5.329	0.592	24	4.5	21
13499636	5518	4.592	11.325	5.595	0.921	17	3.0	15
14091633	6350	4.340	5.529	1.363	0.022	43	31.5	5
14165625	4407	4.563	11.020	8.835	0.908	43	4.9	5,6
20178111	5890	4.488	1.734	4.928	0.675	18	3.7	6
22843856	6019	4.438	1.850	3.518	0.326	19	5.4	18
28230919	4757	4.560	4.888	10.189	1.104	47	4.6	14,15
29191596	5503	4.430	8.819	9.074	1.583	26	2.9	21
33153766	6054	3.473	0.688	2.863	0.186	22	7.7	9
37168957	5440	4.416	1.900	5.248	0.765	18	3.4	6
38541473	5949		6.061	3.009	0.216	21	7.0	4
38603673	6559	3.952	4.428	4.363	0.062	153	35.1	4
44797824	5181	4.145	0.746	1.414	0.022	45	31.8	4,5
47384844	6084	4.130	3.096	3.610	0.310	21	5.8	9
67646988	3138	4.919	1.882	1.105	0.027	23	20.8	21
70797900	3689	4.781		2.037	0.086	24	11.8	2
77031414	6286	4.438	1.387	7.765	1.370	22	2.8	2
77951245	3054	4.438	10.715	5.388	0.338	43	8.0	5,6

NOTE—With one row for each TOI, the following information is listed: the TIC ID, effective temperature (T_{eff}), surface gravity ($\log g$), and orbital period (P_{orb}) taken from the TOI Release Portal (<https://tess.mit.edu/toi-releases/>), rotation period (P_{rot}), error in the rotation period (eP_{rot}), effective time span (t_{SPAN}), and effective number of cycles (N_{Cycle}), obtained from our analysis, and TESS observation sectors. Values for $\log g$ and P_{orb} are rounded to 3 decimals digits.

Table 1. Continue.

TIC ID	T_{eff}	$\log g$	P_{orb}	P_{rot}	eP_{rot}	t_{SPAN}	N_{Cycle}	Sectors
	(K)	(dex)	(days)	(days)	(days)	(days)		
78154865	6030	4.416	0.494	4.634	0.596	18	3.9	8
82128636	6680	4.200	7.474	3.329	0.142	39	11.7	9
92359850	6270	4.140	4.155	3.042	0.231	20	6.6	4
93125144	4692	4.297	9.911	1.427	0.051	20	14.0	6
98796344	3562	4.974	5.359	1.393	0.046	21	15.1	4
102195674	6159	4.377	4.379	4.908	0.574	21	4.3	9
103448870	5734	4.467	10.257	3.103	0.219	22	7.1	19
104024556	7000	4.134	2.022	1.073	0.029	20	18.6	10
117979694	5103	4.610	0.991	8.521	1.513	24	2.8	5
123482865	6845	4.361	13.114	4.330	0.240	39	9.0	8
128790976	6541	4.240	3.519	1.361	0.040	23	16.9	13
130181866	5694	4.531	7.108/20.546	6.508	0.921	23	3.5	20
133334108	5637	4.521	2.854	4.906	0.301	40	8.2	8
138017750	6058	3.840	2.473	2.623	0.181	19	7.2	18
138588540	5394	4.678	29.889	9.236	0.870	49	5.3	14,15
140068425	6174	4.274	2.281	1.064	0.024	24	22.6	1
142090065	7072	4.280	2.828	2.376	0.123	23	9.7	20
142276270	5729	4.470	6.257/12.518/26.322	8.189	0.699	48	5.9	14,15
144401492	4868	4.660	6.294/12.891	4.540	0.448	23	5.1	22
148914726	4928	4.570	1.262	7.391	0.594	46	6.2	14,15
153949511	5544	4.561	37.074	8.095	0.683	48	5.9	14,15
154618248	6208	4.438	8.774	7.599	1.203	24	3.2	2
154716798	5217	4.592	12.640	6.467	0.871	24	3.7	14
154840461	6528	4.210	6.036	5.329	0.302	47	8.8	14,19
154872375	5963	4.380	8.028	5.081	0.281	46	9.1	14,19
156991337	5639	4.400	6.907	3.607	0.155	42	11.6	7
159510109	5895	4.370	16.948	10.045	0.587	86	8.6	14,15
160045097	4336	4.620	4.988	6.071	0.709	26	4.3	21
160074939	6467	4.161	13.340	2.323	0.108	25	10.8	2

Table 1. Continue.

TIC ID	T_{eff}	$\log g$	P_{orb}	P_{rot}	eP_{rot}	t_{SPAN}	N_{Cycle}	Sectors
	(K)	(dex)	(days)	(days)	(days)	(days)		
172464366	6332	4.261	2.922	2.924	0.110	39	13.3	6
173612049	5654	4.520	6.491	4.876	0.305	39	8.0	16,17
176860064	6393		6.376	1.863	0.102	17	9.1	14,15,16
176957796	4651	4.569	4.819	6.197	0.074	260	42.0	1
178284730	5260	4.514	2.236	10.229	1.217	43	4.2	4,5
179034327	5229	4.554	17.963	7.573	0.637	45	5.9	4,5
180695581	4612	4.562	0.549	4.242	0.391	23	5.4	22
183532609	5600	4.505	8.159	7.247	1.094	24	3.3	2
183979262	6270	3.613	3.431	3.341	0.121	46	13.8	1,2
184679932	6198	4.279	2.172	2.175	0.131	18	8.3	18
189013224	5672	4.460	1.321	6.459	0.869	24	3.7	5
190990336	6118	4.290	5.547	3.009	0.216	21	7.0	8
201248411	4486	4.499	0.981	13.219	1.859	47	3.6	2
206609630	3332	4.950	0.335	3.872	0.174	43	11.1	1,2
207141131	5058	4.518	4.137	8.489	0.858	42	4.9	2,3
214361331	7062	4.496	3.231	3.342	0.266	21	6.3	12
219229644	3927	4.697	22.041	9.706	0.748	63	6.5	3,4,5
219776325	5792	4.300	2.529	9.351	0.334	131	14.0	14,15,16,17,18,19
219852882	4992	4.560	1.762/5.503	10.130	0.398	129	12.7	14,15,16,17,18,19
220435095	5808	3.600	3.423	3.538	0.250	25	7.1	1
220459826	4873	4.690	2.240	5.618	0.103	153	27.2	4,5,6
224225541	5862	4.518	4.938	3.773	0.285	25	6.6	2
229747848	5300	4.560	0.847	8.285	0.306	112	13.5	14,15,16
229938290	5406	4.425	1.420	8.603	1.480	25	2.9	21
229951289	5729	4.500	13.312	5.288	0.129	108	20.4	14,15,16,17,18
233211762	5780	4.677	1.122	1.865	0.014	124	66.5	14,15,16,17,18
235037761	4174	4.342	6.241	7.359	1.128	24	3.3	1
238086647	5915	4.128	1.352	2.567	0.055	60	23.4	7
241196395	6436	4.376	2.094	2.019	0.085	24	11.9	21

Table 1. Continue.

TIC ID	T_{eff}	$\log g$	P_{orb}	P_{rot}	eP_{rot}	t_{SPAN}	N_{Cycle}	Sectors
	(K)	(dex)	(days)	(days)	(days)	(days)		
244161191	2955	5.135	0.299	0.321	0.004	14	43.6	3
248092710	6354	4.245	41.465	4.131	0.194	44	10.7	11,10
249945230	4677	4.550		5.749	0.870	19	3.3	18
257605131	5530	4.560	8.186	4.747	0.256	44	9.3	4,5
258777137	5096		5.929	6.364	0.159	127	20.0	14,15,16,17,19
259172391	6240	4.466	9.813	8.132	0.252	131	16.1	14,15,16
271900960	6458	4.430	13.459	1.606	0.005	285	177.5	4
277683130	5722	4.356	6.198	8.543	1.520	24	2.8	1
278198753	4320	4.572	7.943	4.015	0.322	25	6.2	12
278683844	5332	4.564	5.541/10.692	10.408	0.203	267	25.7	1,2,3,4,5,6,8,9,10,11,12,13
279425357	6084	4.320	9.014	3.802	0.168	43	11.3	9
280830734	6340	4.180	1.162	3.633	0.135	49	13.5	1,2
281924357	5900	4.363	15.042	4.020	0.115	70	17.4	11
281979481	5181	4.546	0.542	4.385	0.084	114	26.0	3
288631580	5977	4.470	5.877	6.934	0.359	67	9.7	18,19
293954617	5064	4.579	7.434	5.368	0.203	71	13.2	15
299158887	5450	4.480	9.435	5.267	0.578	24	4.6	14
299798795	3442	4.893	4.178	1.166	0.014	49	42.0	13,1
300293197	5874	4.352	6.564	5.999	0.063	285	47.5	1,2,3
307610438	5808	4.340	1.562	3.290	0.338	16	4.9	11
309257814	5237	4.243	1.239/1.814	3.948	0.390	20	5.1	10
309402106	7053	4.225	216.245	5.393	0.109	133	24.7	1,5,8,9,10,11
310009611	5776	4.406	2.130	5.091	0.288	45	8.8	9,10
311183180	5076	4.710	10.043/13.250	8.764	1.670	23	2.6	5
312862941	3810	4.569	0.915	1.779	0.079	20	11.2	18
318937509	3109	5.066	1.049	2.005	0.096	21	10.5	7
320004517	5784	4.499	17.471	8.600	1.422	26	3.0	13
327017634	3773	4.438		2.552	0.068	48	18.8	11,12
335630746	6780	4.082	4.634	2.531	0.160	20	7.9	10

Table 1. Continue.

TIC ID	T_{eff}	$\log g$	P_{orb}	P_{rot}	eP_{rot}	t_{SPAN}	N_{Cycle}	Sectors
	(K)	(dex)	(days)	(days)	(days)	(days)		
339961200	5321	4.510	3.213	9.670	0.277	169	17.5	6,7,8
344926234	5872	4.440	0.494	6.112	1.038	18	2.9	8
352239069	6052	4.480	6.868	3.303	0.077	71	21.5	14,15,16
356311210	5897	4.459	18.056	5.356	0.231	62	11.6	14,17,18
356867115	4820	4.600	6.096	12.587	0.619	128	10.2	14,15,16
357457104			1.748	3.684	0.188	36	9.8	15,16
360156606	3050	4.438	27.361	1.663	0.028	49	29.5	11,12
380783252	5509	4.398	9.450	9.147	1.609	26	2.8	13
382391899	5400	4.539	1.955	5.488	0.753	20	3.6	4
382474101	6054	4.290	2.652	2.722	0.168	22	8.1	2
383390264	6153	4.348	10.185	2.149	0.044	52	24.2	13
387260717	6009	4.640	6.451	4.128	0.101	84	20.3	16,17,18,19
389070884	5963	4.438	8.584	5.391	0.692	21	3.9	12
406976746	5552	4.618	10.065	7.485	0.539	52	6.9	12,13
410214986	5414	4.438	8.138	2.798	0.163	24	8.6	1
422923265	9898	3.778	1.865	7.738	1.576	19	2.5	18
441732151	6025	4.460	2.100	2.002	0.020	102	50.9	15,16,17,18,19
447283466	4691	4.640	1.016	9.501	1.003	45	4.7	9
451645081	4499	4.500	16.234	5.569	0.705	22	4.0	10
459970307	5671	4.510	21.748	3.581	0.049	130	36.3	14,15,16,17,18,19,20
460205581	6513	4.537	8.325	2.957	0.093	47	15.9	11
461271719	7313	4.144	15.246	3.822	0.406	18	4.7	11
462162948	9488	4.075	19.847	5.508	0.337	45	8.2	9

Table 2. List of the 32 TOIs with dubious rotation periods from our analysis.

TIC ID	T_{eff}	$\log g$	P_{orb}	P_{rot}	t_{SPAN}	N_{Cycle}	Sectors
	(K)	(dex)	(days)	(days)	(days)	(days)	
1129033	5500	4.483	1.360	5.00/10.00	19	1.9	4
1528696	4975	4.520	0.882	5.15/8.97	23	2.6	5
9006668	5024	4.569	1.272	7.05/9.96	25	2.5	2
35516889	5568	4.393	0.789	6.18/9.37	19	2	9
36734222	4400	4.646	0.813	7.40 ^a	19	2.6	9
62483237	4356	4.535	11.058	6.83/11.09	24	2.2	1
77044471	5738	4.238	2.686	11.28 ^a	23	2	2
101011575	4695	4.500	6.397	7.17 ^a	18	2.5	8
101948569	4333	4.511	19.472	8.81 ^a	24	2.7	2
112395568	5664	3.266	5.743	10.78 ^a	23	2.1	13
131081852	6072	4.292	13.274	7.14 ^a	21	2.9	10
142394656	5091	4.470	8.158	6.21/9.42	23	2.4	15
150151262	4504	4.588	9.532/51.705/53.746	6.07/11.33	172	15.2	3,4,6,7,9
150428703	5523	4.672	13.896	4.52/7.34	204	27.8	4,5,6,7,9,10,11,12,13
179308757	5780	4.138	0.966	5.09/8.87	193	21.8	2,3,4,5,6,7,8,9
198384408	5470	4.300	9.124	9.81/15.94	109	6.8	19
233071926	4837	4.517	1.832	5.34/9.30	24	2.6	14,15,16,17,18,19
233120979	5273	4.438	5.963	4.24/8.48	109	12.9	14,15,16
241225337	5566	4.440	1.833	5.32/9.93	24	2.4	20
262530407	3703	4.762	2.853	5.21/11.17	42	3.8	2,3
277099925	5780	4.438	0.809	4.00/5.28/8.58	240	28	1,3,4,6,7,8,9
286132427	5914	4.465	0.493	5.71/13.13	18	1.4	8
286864983	5184	4.574	11.018	3.30/7.08	21	3	10
290348383	4867	4.438	6.442	5.55/11.11	26	2.3	13

NOTE—The following information is listed: the TIC ID, effective temperature (T_{eff}), surface gravity ($\log g$), and orbital period (P_{orb}) taken from the TOI Release Portal (<https://tess.mit.edu/toi-releases/>), likely rotation period values (P_{rot}), effective time span (t_{SPAN}), and effective number of cycles (N_{Cycle}), obtained from our analysis, and *TESS* observation sectors. Flag *a* corresponds to stars with less than three observed cycles that show non-persistent pattern along their LCs. Values for $\log g$ and P_{orb} are rounded to 3 decimal digits.

Table 2. Continue.

TIC ID	T_{eff} (K)	$\log g$ (dex)	P_{orb} (days)	P_{rot} (days)	t_{SPAN} (days)	N_{Cycle} (days)	Sectors
298647682	4763	4.543	40.158	5.27/10.54	68	6.5	14,15
310981412	6149	4.570	9.625	4.94/6.98	76	10.9	14,20,21
328350926	5625		0.849	5.63/9.80	19	1.9	4
360742636	5659	4.447	2.550	2.78/5.55	25	4.5	13
362249359	3965	4.683	1.042	4.01/7.49	67	8.9	11
367753709	4428	4.580	2.126	10.09 ^a	23	2.3	14,15,18,19
405700729	6012	4.767	4.794	8.53 ^a	22	2.6	11
458589703	4788	4.590		9.42 ^a	22	2.3	7

Table 3. List of the 109 TOIs with ambiguous variability behavior from our analysis.

TIC ID	T_{eff}	$\log g$	P_{orb}	t_{SPAN}	Sectors
	(K)	(dex)	(days)	(days)	
1003831	5752	4.471	1.651	18	8
1103432	6231	4.264	3.728	17	8
4646810	4884	4.490	14.490	21	4
9804616	3274	4.979	0.517	19	4
12862099	5410	4.479	2.424	17	3
13684720	3275	4.758	12.438	36	14,15
15445551	6271	4.082	1.683	39	10
16288184	6599	4.210	2.181	19	12
16740101	9435	4.110	1.481	31	14,15
17005768	5766	4.438	6.843	17	17
19025965	4383	4.565	5.948	21	7
22221375	5903	4.447	3.985	21	9
22529346	6459	4.240	1.275	19	7
25375553	6371	3.948	2.311	22	1
29191624	5859	4.478	14.653	26	21
30312676	8747	4.080	1.102	225	11
30828562	7850	4.087	3.112	38	8
31374837	4771	4.620	0.490/12.459	43	5,6
31553893	5785	4.344	11.113	24	13
31852980	5450	4.410	7.414/24.333	135	1,2,3,6
31858843	5703	4.258	2.978	22	13
31858844	5740	4.292	2.978	22	13

NOTE—The following information is listed: the TIC ID, effective temperature (T_{eff}), surface gravity ($\log g$), and orbital period (P_{orb}) taken from the TOI Release Portal (<https://tess.mit.edu/toi-releases/>), effective time span (t_{SPAN}) obtained from our analysis, and TESS observation sectors. Values for $\log g$ and P_{orb} are rounded to 3 decimals digits.

Table 3. Continue.

TIC ID	T_{eff}	$\log g$	P_{orb}	t_{SPAN}	Sectors
	(K)	(dex)	(days)	(days)	
32090583	3146	4.438	0.438	243	1,2,3,4,6
32830028	3009	5.110	0.516	19	6
34068865	3518	4.825	0.322	22	9
37749396	4111	4.646	13.470	18	3
44631965	6046	4.269	3.569	17	17
47911178	6400	4.344	3.586	19	6
48476907	6521	4.220	4.720	20	9
48476908	5990	4.010	4.720	20	9
49899799	6085	4.010	7.012	20	4
50618703	4665	4.676	1.548	20	6
58542531	4402	4.590	3.058	22	19
64071894	5164	4.537	17.530	21	4
67666096	6518	4.150	2.703	23	21
73723286	6157	4.204	14.066	21	9
76923707	4983	4.614	4.532	24	2
76989773	5569	4.321	1.769	23	2
79748331	4803	4.521	6.442/12.226	24	13
85242435	6137	4.430	9.607	23	20
85293053	5583	4.440	8.051	23	21
89256802	3054	5.090	1.176	20	4
96097215	5272		1.602	18	8
101230735	5688	4.600	2.069	24	13
122612091	6250	3.988	2.217	35	4,3
125442121	7128	4.238	3.020	20	16
144065872	5630	4.348	12.837	22	1
140830390	5765	4.378	2.185	71	13
147660201	5688	4.488	0.579	35	9
148228019	7403	4.138	18.089	41	6
148782377	6383	4.245	14.419	21	16

Table 3. Continue.

TIC ID	T_{eff} (K)	$\log g$ (dex)	P_{orb} (days)	t_{SPAN} (days)	Sectors
149603524	6280	4.321	4.412	249	1,2,3,4,6
151825527	3765	4.752	3.634	42	9
153077621	3321	4.954	18.083	39	3,4
158297421	4444	4.438	3.923	24	13
159418353	4814	4.545	8.304	23	14,19
167415965	5346	4.600	9.696/18.553	271	13,12,11,10,9,7,5,6,4,3,2,1
176831592	6498	4.170	1.267	19	4
176984236	6249	4.280	1.756	191	4
177077336	4908	4.578	1.418	243	2,3,4,5,6
177244357	5772	4.390	6.547	17	17
190998418	5583	4.339	2.879	17	17
199688472	5673	4.130	1.441	119	14,15,16,17,19
200322593	3042	4.438	1.239	64	4,5,6
200723869	6050	4.050	18.371	39	4
201793781	5712	3.840	5.991	43	2,3
219698776	3489	4.746	4.663	25	14
231663901	5600	4.489	1.430	23	1
233071822	4435	4.589	2.755	23	14,15,16,17,18,19
233390838	6478	4.130	6.448	64	15,16
234519192	6495	3.320	1.163	25	2
234994474	3794	4.678	1.401	24	1
236887394	4910	4.572	1.420	19	17
237086564	4201	4.508	1.872	19	17
237200747	5057	4.530	14.304	129	15
238898571	5867	4.595	0.525	66	5,6
256783784	5459	4.510	6.112	39	16
260128333	5723	3.600	71.417	175	4,5,6,7,8,9,10,11,12
261108236	4310	4.573	16.348	51	13
261257684	3992	4.619	18.352	51	12

Table 3. Continue.

TIC ID	T_{eff}	$\log g$	P_{orb}	t_{SPAN}	Sectors
	(K)	(dex)	(days)	(days)	
266593143	5337	4.555	10.338	17	15
269892793	4769	4.648	1.773	19	18
283722336	4884	4.590	3.093/6.765	20	17
286923464	5829	3.840	6.135	44	15,16
293617835	6096	3.260	2.757	23	20
298372701	5955	3.686	1.665	20	12
304100538	5551	4.462	5.010	51	1,13
308034948	5824	4.438	0.832	44	10,11
308307606	5522	4.395	15.003	82	7
317507345	7170	4.310	3.940	19	18,19
325680697	5773	3.510	1.825	20	4
326919774	8756	3.450	7.572	38	17
329864959			4.523	39	16,17
348538431	3338	4.947	0.899	20	7
350445771	6475	4.264	3.190	276	1,2,3
350584963	6623	4.384	2.126	267	1,2,3,4,5,6,7,8
352413427	5958	4.482	5.255	17	17
364395234	5739	4.282	14.259	83	9,10,11,13
373844472	5616	4.376	0.919	215	3,1
375542276	9311		3.078	18	14
387259626	6459	4.320	3.623	39	15,16,17
391821647	6636	4.605	1.996	267	1,2,3,4,5,6
391949880	6086	4.263	4.941	116	1
394657039	6404	4.220	3.763	25	1
398943781	5545	4.528	3.052	20	10
427352241	6084	4.290	1.265	18	6
440887364	4476	4.582	3.817/8.594	18	11
445805961	5675	4.460	24.283	23	20
1884091865	4067	4.506	10.691	130	19,20

Table 4. List of the 714 TOIs with noisy LCs in our analysis.

TIC ID	T_{eff}	$\log g$	P_{orb}	t_{SPAN}	Sectors
	(K)	(dex)	(days)	(days)	
1133072	3380	4.925	0.847	15	8
1449640	6383	4.030	3.502	23	5
4616072	6675	4.201	4.186	40	6
4897275	5854	4.386	16.710	24	21
5868998	3602	4.817	0.636	18	10
6663331	5498	4.479	3.180	23	13
7088246	5780	4.329	2.160	23	13
8400842	6673	4.130	3.192	22	19
8767448	5914	4.070	4.353	23	21
9725627	6363	4.590	4.157	23	2
9858404	6216	3.730	0.391	21	4
11561667	4105	4.438	3.088	20	9
12421862	3763	4.837	20.427	24	2
12423815	3642	4.438	2.839	24	2
13021029	6407	4.210	3.856	22	5
13349647	5959	4.489	1.537	17	8
14091704	3151	3.970	0.765	22	5
14336130	5878	4.280	8.088	24	20
14614418	5600	4.438	0.838	18	10
14661418	4803	4.642	4.723	20	10
15863518	5098	4.420	0.557	20	20
16920150	5219	4.557	9.156	17	17

NOTE—The following information is listed: the TIC ID, effective temperature (T_{eff}), surface gravity ($\log g$), and orbital period (P_{orb}) taken from the TOI Release Portal (<https://tess.mit.edu/toi-releases/>), effective time span (t_{SPAN}) obtained from our analysis, and TESS observation sectors. Values for $\log g$ and P_{orb} are rounded to 3 decimals digits.

Table 4. Continue.

TIC ID	T_{eff}	$\log g$	P_{orb}	t_{SPAN}	Sectors
	(K)	(dex)	(days)	(days)	
17746821	6280	4.081	3.122	20	7
19451711	7381	4.438	0.398	22	7
19519368	4985	4.670	1.702	22	7
21535395	5724	4.495	2.801	26	21
23434737	5742	4.290	25.492	43	9,10
25155310	5800	4.280	3.289	269	1,2,3,4,5,6
27649847	3439	4.975	1.542	21	7
28900646	3457	4.771	0.669	23	19
29054413	5473	4.465	7.626	20	18
29344935	5346	4.488	2.767	23	1
29781292	6321	4.224	31.323/56.011/84.216	288	1,2,3,4,5,6,7,8,9,10,11,12,13
29831208	5080	4.482	1.843	250	3,1
29960109	3856	4.780	2.492	20	4
29960110	3948	4.690	2.491	20	4
30037565	5914	3.980	40.720	288	1,2,3,4,5,6,7,8,9,10,11,12,13
30122649	5216	4.526	9.736	40	9,8
30853470	4662	4.568	5.270	266	1,2,3,4,5,6,7,8
32497972	3955	4.689	38.696	43	5,6
32499655	4860	4.438	2.744	43	5,6
33521996	3724	4.683	3.325	19	6
33692729	6114	4.510	13.633	19	6
33831980	4130	4.438	21.916	200	1,2,3,5,6,8,9
33878688	5168	4.606	79.367	265	1,2,3,5,6,7,8,9,10,11,12,13
35009898	3433	4.897	1.527	20	9
35857242	6272	4.258	3.635	20	4
36352297	5950	4.326	1.509	18	6
36440357	6190	4.367	9.199	19	6
36724087	3329	4.950	0.768/12.254	20	9
37575651	5780	4.438	9.596	18	8

Table 4. Continue.

TIC ID	T_{eff} (K)	$\log g$ (dex)	P_{orb} (days)	t_{SPAN} (days)	Sectors
37770169	5418	4.573	12.194	20	6
38460940	3376	4.438	4.118	170	8,7,5,4,3,1
38509907	4082	4.632	15.299	236	5,4,3,2,1
38510224	4356	4.605	18.383	196	8,7,5,4,3,2,1
38571020	6009	4.218	12.289	285	5,6,4,3,2,1
38686737	6846	4.230	2.247	22	5
38696105	6002	4.124	5.567	65	3
38846515	6900	4.438	2.849	265	5,6,4,3,2,1
39699648	6023	4.240	6.516	23	21
41227743	5988	4.307	1.418	224	8,7,5,6,4,2,1
42054565	5454	4.591	10.176	18	3
42821097	6090	4.086	3.895	18	6
43064903	3145	5.044	6.264	17	15
43647325	5904	4.410	3.162	22	5
44647437	3978	4.438	3.353	43	5,4
44737596	3654	4.438	2.789	43	5,4
44745077	3550	4.870	1.876	43	5,4
46096489	5700	4.492	3.119	18	11
47316976	6446	3.960		24	2
47484268	3396	4.915		24	2
47525799	4658	4.531		24	2
48103627	6122	4.283	4.570	20	9
49687222	6101	4.482	20.187	24	2
49771092	5084	4.481	1.631	19	6
50309953	5317	4.490	7.041	49	13,1
50312495	5573	3.830	14.707	51	13,2
51024887	2990	5.136	8.249	19	18
51234631	6304	4.110	4.125	22	20
51912829	6082	3.777	0.835	44	2,1

Table 4. Continue.

TIC ID	T_{eff} (K)	$\log g$ (dex)	P_{orb} (days)	t_{SPAN} (days)	Sectors
52204645	4892	4.510	4.380	48	2,1
52280468	3294	4.438	0.568	37	6
52368076	5154	4.471	4.654/9.151/19.982	47	2,1
52640302	5400	4.388	1.573	38	6
53189332	6055	4.228	9.290	20	9
53593457	3085	5.080	0.531	16	6
53735810	6580	4.066	4.087	20	9
54085154	6380	4.438	1.001	21	9
54962195	3719	4.769	2.599/4.698	20	9
55092869	5370	3.728	4.736	19	9
55383975	5355	4.459	48.052	219	5,6,4,1
55452495	7859	4.120	8.857	117	2
55488511	3883	4.710	3.345	23	5
55525572	5824	3.770	83.899	195	9,8,5,6,4
55559618	5591	4.381	21.375	284	5,6,4,3,2,1
55650590	3358	4.438	0.736	271	5,6,4,3,2,1
55652896	5026	4.663	17.082/34.549	258	5,6,4,3,2,1
59003115	5062	4.620	2.294	24	5
59843967	5403	4.501	2.517	19	6
61538902	5900	4.530	5.748	21	10
61988212	5591	4.381	0.555	18	10
63898957	5890	3.920	3.361/13.039	18	3
66818296	6650	4.164	3.735	20	12
67418624	6011	4.040	1.104	20	18
69679391	8895	4.380	3.474	17	14
69747919	6074	4.100	9.979	25	2
70440470	5751	4.350	3.035	23	1
70513361	5303	4.535	11.147	18	3
70899085	4101	4.640	4.052	24	5

Table 4. Continue.

TIC ID	T_{eff}	$\log g$	P_{orb}	t_{SPAN}	Sectors
	(K)	(dex)	(days)	(days)	
70914192	5272	4.340	0.610	21	5
71431780	5777	4.380	13.716	23	20
71512186	7064	4.224	14.822	20	6
72985822	6214	4.267	3.864	21	10
73228647	6003	4.474	2.540	22	10
73649615	3614	4.813	1.239	41	10
73717937	5846	4.417	16.258	43	11
74534430	4254	4.570	18.155	39	9,8
77156829	3450	4.890	0.860/14.776	45	5,4
77228304	5780	4.438	0.337	38	5,4
77253676	5447	4.400	8.607	45	5,4
78055054	5175	4.465	4.389	42	5,6
81212286	3541	4.845	0.685	21	20
82362447	3601	4.819	2.820	15	8
83092282	7056	4.334	6.402	38	8
85031598	4815		1.155	23	19
86396382	6154	4.020	1.091	18	20
88977253	6717	4.200	2.768	21	7
89020549	5673	4.554	2.109	23	1
90504905	3443	4.816	2.265	16	14
92226327	3131	5.057	3.778/24.737	18	3
92352620	6153	4.181	3.950	23	1
94986319	5718	4.357	16.069	43	5,6
97409519	6050	4.451	3.373	23	1
99834717	4974	4.441	1.706	23	21
100608026	4105	4.600	8.260	43	5,6
100990000	6101	4.388	4.040/9.572	39	4,3
101395259	6422	4.206	15.151	38	8

Table 4. Continue.

TIC ID	T_{eff}	$\log g$	P_{orb}	t_{SPAN}	Sectors
	(K)	(dex)	(days)	(days)	
101497191	5463	4.390	3.644	20	9
101955023	3202	4.864	1.629	41	9
102672709	6141	4.176	6.702	23	19
103633434	3912	4.626	3.443	25	20
106402532	5969	4.517	4.887	21	9
108645766	3333	4.948	2.974	21	7
110428269	8809	4.020	0.650	18	14
111991770	6300	4.170	3.752	18	11
115771549	6112		4.718	20	16
116483514	4184	4.574	1.452	23	16
116483734	4223	4.617	4.732	22	16
117979455	5795	4.220	0.633	23	5
117979850	5713	3.670	0.633	24	5
117979897	5928	4.220	3.311	22	5
118327550	3342	4.438	7.396	24	2
119081096	3776	4.720	0.837	15	8
119292328	5581	4.522	7.187	42	7
119700084	5427	4.515	6.117	21	16
120247528	5639	4.372	3.554	25	13
120585579	6083	4.290	6.340	24	2
120602501	5705	3.970	7.431	21	16
120610833	5100	4.465	3.126	24	2
120757718	5243	4.524	3.030	17	14
120896927	5175	4.377	4.756/17.215	39	4
120916706	3116	5.060	0.557	16	3
120960812	6212	4.177	12.726	25	14
121338379	6218	4.267	0.275	22	7
121966220	5843	3.718	6.717	21	19
122220263	6113	4.090		17	14

Table 4. Continue.

TIC ID	T_{eff} (K)	$\log g$ (dex)	P_{orb} (days)	t_{SPAN} (days)	Sectors
122613513	4140	4.463	11.494	38	4,3
123702439	5997	4.457	8.521	39	7
124573851	5582	4.130	3.949	21	9
125405602	3669	4.789	13.823	18	11
126733133	5973	4.273	1.469	17	8
127530399	4775	4.603	14.267	18	11
130924120	5499	4.400	17.466	21	10
131419878	6842	4.210	3.160	40	8
134200185	4590	4.510	0.548	60	7
134537478	5720	4.168	1.710	20	7
137881699	6101	3.920	2.972	24	21
137906197	5994	4.400	7.339	25	21
138168780	6724	4.290	3.765	21	19,20
138968089	5865	4.126	0.641	38	15
139528693	6317	3.900	2.175	21	5
139733308	5220	4.510	4.764	23	5
140691463	5391	4.350	2.085	91	1
140760434	6029	3.962	31.814	72	13,12,11
141527579	3570	4.832	15.087	265	5,4,3,2,1
141527965	4280	4.612	4.554	267	13,12,11,10,9,8,7,5,4,3,2,1
141608198	3275	4.438	9.010	263	5,4,3,2,1
141768070	5376	4.425	2.786	92	11
143271144	4978	4.438	1.353	18	6
143350972	5729	4.450	1.082	44	5
143526444	5370	3.323	15.302	40	8,7
144138509	6023	4.050		21	9
144440290	5709	4.438		25	2

Table 4. Continue.

TIC ID	T_{eff}	$\log g$	P_{orb}	t_{SPAN}	Sectors
	(K)	(dex)	(days)	(days)	
144700903	3946	4.690	2.327	19	6
146463781	3278	4.978	0.418	30	8
146846569	3010	5.110	4.753	42	9
147950620	5340	4.410	2.311	24	14,20
148479278	7450	4.340	0.523	42	7
149301575	5804	3.890	183.459	285	9,8,7,5,6,4,3,2,1
149302744	6139	4.070	14.801/33.621	269	5,6,4,3,2,1
149788158	3476	4.740	4.726	18	8
149990841	5766		4.453	67	1
150030205	5245	4.577	4.512/39.361	268	13,12,11,10,9,8,7,5,4,3,2,1
150098860	5273	3.988	10.695	243	12,11,10,9,8,7,5,6,4,2,1
150247134	4938		12.863	104	8
150271680	5317	3.880	2.594	268	9
150428135	3482	4.438	9.977/16.051/37.425	238	9,8,7,5,6,4,3,1
151681127	7949	4.211	10.198	21	9
151959065	6114	4.284	10.541	41	9
152147232	6107	4.116	4.213	20	10
152476657	6450	4.038	3.611	43	5,4
153065527	3349	4.941	13.174	39	4,3
153951307	3853	4.632	0.765/3.294	47	14,15
153976959	5142	4.546	0.686	49	14,15
154089169	5030	4.610	8.953	48	14,15
154383539	5011	4.614	0.867	47	15,16
155114483	8110	4.320	5.265	17	16,17
158002130	4738	4.590	9.692	46	14,19
158025009	4946	4.538	1.070	22	16
158170594	5833	4.209	1.721	23	14
158324245	7986		1.764	43	14,15
158561566	6378	4.438	6.791	46	14,15

Table 4. Continue.

TIC ID	T_{eff}	$\log g$	P_{orb}	t_{SPAN}	Sectors
	(K)	(dex)	(days)	(days)	
158588995	3467	4.879	1.977	42	9
158623531	5070	4.479	7.873	41	3,2
158978373	6309	4.235	13.539	18	11
159107668	5826	3.721	4.780	48	14,15
159951311	5310	4.596	5.924	38	4,3
160148385	5540	4.421	3.425	24	2
161032923	3296	4.966	3.965	23	13
161477033	5465	4.570	11.928/14.058/40.902	45	5,4
162362398	7852	4.204	12.352	20	10
163539739	3841	4.694	14.476	17	15
164767175	5784	4.438	6.191/10.768	18	3
165317334	4368	4.567	10.563	21	10
165551882	3429	4.901	12.158	108	18
166739520	6038	4.355	10.021	41	3,2
166833457	5473	4.608	2.962	20	4
166836920	6180	4.118	5.752	17	3
167303382	5236	4.438	3.694	266	13,12,11,10,9,8,7,5,6,3,2,1
167342439	5409	4.462	52.809	268	5,6,4,3,2,1
167418898	6077		10.980	265	4
167418903	5517	4.470	10.980	74	8,7,4,3
167600516	4317	4.609	1.872/36.000	267	8,7,5,6,4,3,2,1
167754523	4914	4.540	1.700	289	4
169226822	5620	4.186	4.178	20	9
169532369	6897	4.170	3.604	23	5
170102285	5150	4.558	2.944	19	6
170634116	6600	4.209	3.662	42	5,4
170849515	3837	4.726	1.941	22	5
172193428	5642	4.167	2.942	21	7

Table 4. Continue.

TIC ID	T_{eff}	$\log g$	P_{orb}	t_{SPAN}	Sectors
	(K)	(dex)	(days)	(days)	
174143743	6121	4.410	0.461	18	8
175180796	4147	4.600	1.557	36	8,7
176778112	5600	4.437	1.339	21	4
177115354	5668	4.526	3.929	131	13,10,8,7,5,6
177162886	5591	4.307	12.846	116	12
177258735	6283	4.438	0.776	265	13,12,11,10,9,8,7,6,4,3,2,1
178155732	6308	4.438	3.587/5.969/11.232	21	4
178709444	3399	4.915	3.472	20	10
178819686	5767	4.347	5.605/12.276	22	10
179317684	6388	4.140	4.231	110	1
179985715	4157	4.593	6.613	24	2
181159386	6632	4.206	5.632	20	10
181804752	2940	5.143	0.948/4.990	21	9
183120439	5781	4.230	2.256	25	1
183537452	4800	4.535	3.923	24	2
183985250	5422	4.422	0.792	23	2
184240683	5700	4.395	1.628	23	2
184952758	5761	4.460	4.106	18	8,7
186599508	5670	4.160	5.632	19	18
186812530	7887	4.281	3.677	21	7
188768068	5802	4.251	2.178	18	17
188989177	7765	3.610	1.174	22	5
191284318	6030	4.320	2.776	16	17
192826603	3916	4.719	2.647	43	5,6
193641523	4452	4.499	1.393	46	11
198206613	4324	4.697	10.942	23	14,15,16,17,18,19
198212955	4255	4.556	0.381	130	14,15,16
198213332	5874	3.670	0.586	47	14,15,16,17,18,19
198241702	5591	4.381	4.253/9.239	129	14,15,16,17,18,19

Table 4. Continue.

TIC ID	T_{eff} (K)	$\log g$ (dex)	P_{orb} (days)	t_{SPAN} (days)	Sectors
198356533	6093	4.322	18.840	131	14,15,16
198390247	4920	4.640	4.313/6.589	112	14,15,16,17,19,20
198457103	7141	4.080	0.472	130	14,15,16,17
199376584	6043	4.290	12.156	35	15
199444169	4635	4.510	1.217	20	16
200593988	3617	4.811	7.699	19	6
200807066	5908	4.282	26.477	39	4,3
201186294	3455	4.768	0.989	19	18
201642601	4351	4.438	3.131	25	13
204317710	5700	4.397	2.812	23	2
204376737	5375	4.494	3.361	24	2
206466531	6000	4.360	1.427	39	4
207081058	6053	4.314	14.775	24	1
207084429	5883		4.894	43	2
210873792	3861	4.718	4.844	20	12
211438925	5940	4.232	4.899	24	2
216935214	7142	4.157	18.262	21	12
218795833	3225	5.005	1.265	21	7
219164808	6915	4.176	1.677	42	7
219187649	5430	4.414	2.150	20	9
219189765	3394	4.919	1.732	20	9
219195044	3782	4.438	4.323/10.177	153	8,7,5,6,4
219239945	5837	4.377	13.697	62	5,4,3
219253008	5868	3.573	5.066	59	5,4,3
219338557	4028	4.559	8.195	24	1
219344917	4939	4.585	28.694	65	5,6,4
219345200	5710	3.530		65	5,6,4
219379012	5974	3.890	1.547	39	4
219388773	4753	4.370	1.571	65	4

Table 4. Continue.

TIC ID	T_{eff} (K)	$\log g$ (dex)	P_{orb} (days)	t_{SPAN} (days)	Sectors
219401954	5725	3.820	0.861	130	10
219698950	5870	4.400	3.447	20	10
219850915	4599	4.585	6.398	108	14,15,16
219857012	5707	4.319	21.272	23	15,16,17,18,19
219860288	3281	4.904	4.266	23	15,16,17,18,19
220029715	4944	4.502	3.185	18	11
220396259	5825	4.040	0.917	89	2
220459976	3891	4.640	32.333	220	3,2
220475245	4833	4.517	3.782	50	12
220479565	3607	4.438	3.698	128	5,6,4,3
224297258	5477	4.571	9.615	23	15
224596152	5773	4.462	28.872	23	14,15,16,17,18,19
224600500	8475	3.822	0.676	131	14,15,16,17,18,19
229047362	5703	4.511	3.765	20	10
229455001	6179	4.397	22.342	23	14,15,16,17,18,19
229650439	5374	5.961	5.140/9.427	130	14,15,16,17,18,19
229770036	4567	4.390	2.141	112	16
229781583	3692	4.716	4.821	128	14,15,16
229811538	5956	4.313	11.529	21	10
229940491	5730	4.098	37.460	110	14,15,16,17,18
229944666	5290	4.533	11.328	130	17
230017324	4665	4.562	9.692	130	14,15,16,17
230086768	3496	4.900	8.858	102	18
230088370	6558	4.180	14.008	104	14,15,17,18,19
230127302	5141	4.491	4.307/5.903/18.652	109	14,15,16
230377505	5617	4.470	4.516	23	20
230982885	5640	4.437	2.073	23	2
231081369	6338	4.160	7.632	115	1
231670397	6036	3.934	4.087	22	1

Table 4. Continue.

TIC ID	T_{eff}	$\log g$	P_{orb}	t_{SPAN}	Sectors
	(K)	(dex)	(days)	(days)	
231702397	3318	4.958	5.078	24	1
231728511	3460	4.438	0.521	65	5,6,4
231912935	5821	4.441	26.297	49	2,1
232025086	6437	4.247	5.902	66	5,6
232540264	5712	4.383	15.924	71	14,15,16
232612416	5227	4.505	4.360	126	14,15,16,17,18
232967440	5430	4.440	7.064	48	14,15
232971294	6191	4.270	6.391	49	14,15,20
232976128	5453	4.417	13.078	48	14,15
232982558	5873	4.043	27.643	129	14,15,16
233009109	6669	4.010	14.447	23	15,16,17,18,19
233059608	6603	4.438	1.442	130	14
233087860	4681	4.610	5.748	131	14,15,16,17,18,19
233541860	4154	4.530	0.267	132	14,15,16,17
233602827	3959	4.684	4.489/9.046	23	14,15,16,17,18,19
233617847	5780	4.438	15.517	110	14,15,16
233681149	5929	4.483	8.587	124	14,15,16,17,18
233684293	6153	3.720	48.479	25	21
233684822	5779	4.882	4.676	129	14,15,16,17,18
233735068	5147		7.687	128	14,15,16,17,19
233951353	5885	4.278	22.096	91	14,15,16
234112540	6100	4.287	4.038	19	6
234345288	4566	4.930	23.520	75	13,2,1
234523599	3424	4.438	3.796	47	2,1
234825296	5880	4.478	9.246	20	6
235683377	3328	4.916	0.409	118	14,15,16
236445129	6430	4.251	0.969	15	15
236714379	5451	4.339	1.018	99	14,15,16,17,18
237099296	4765	4.551	11.338	23	14,16,17,18,19

Table 4. Continue.

TIC ID	T_{eff}	$\log g$	P_{orb}	t_{SPAN}	Sectors
	(K)	(dex)	(days)	(days)	
237222864	5126	4.498	10.289	111	14,15,16,17,19
237232044	5236	4.639	23.541	108	14,16,17,18,19
237751146	3411	4.909	1.670	18	6
237914496	4015	4.615	3.568	129	4,3,2,1
237920046	3797	4.740	5.931	107	4,3,2,1
237924601	5071	4.483	1.002	62	3,2
237928815	5384	4.548	8.673/45.120	64	4,2
238004786	4186	4.450	0.310	109	6
238176110	4920	4.494	2.799	23	1
238197638	6266	4.270	14.543	51	12
238197709	5772	3.960	13.725	51	
238932509	5153	4.469	3.493	46	11
239154970	6642	4.140	3.474	20	20
240681314	6695	4.175	2.733	17	17
240968774	3834	4.746	5.973	37	17
243185500	3382	4.855	1.880/15.532	17	17
243200602	5625	4.491	11.552	22	11
248075138	5315	4.517	4.982	21	10
248111245	6438	4.110	4.636	41	10
250386181	6321	4.198	1.470	20	4
251848941	4111	4.555	6.558/9.956/10.354	24	2
252479260	5358	4.370	3.212	25	21
253728991	6027	4.300	2.983	23	13
253990973	5525	4.253	0.541	24	13
255685030	5643	4.481	5.545	110	5,6,7,8,12
255760319	5920	3.910	7.210	60	8,6
256886630	8494	3.940	2.039	39	15
257241363	5378	4.460	5.587	21	20
257567854	6153	4.342	3.533	20	4

Table 4. Continue.

TIC ID	T_{eff}	$\log g$	P_{orb}	t_{SPAN}	Sectors
	(K)	(dex)	(days)	(days)	
258514800	5466	4.486	0.470	108	15,16,19
259168516	3231	5.041	4.802	130	14,15,16
259377017	3551	4.840	3.360/5.660/11.380	62	5,4,3
259511357	6025	4.331	2.476	63	5,4,3
259592689	5160	4.430	14.804	80	5,4,3
259701242	5928	4.480	2.486	109	4
259863352	5625	4.438	21.702	75	13
259962054	3203	5.017	51.953	66	2,1
260004324	3625	4.783	3.814	268	5,4,3,2,1
260043723	6278	4.082	3.139	288	2,1
260130483	5556	3.930	88.934	74	10,8,4
260271203	5963	4.311	5.650	273	4
260304296	6725	4.195	0.513	233	2,1
260304800	5324	4.436	3.441	111	9
260476837	4814	4.519	2.233	69	12
260609205	6354	4.245	4.462	268	2,1
260640693	4270	4.578	95.245	245	9,8,7,5,6,4,1
260647166	5724	4.438	3.795/6.203/14.176/19.593	44	11,10
260708537	3445	4.852	1.745	267	13,12,11,10,9,8,5,6,4,3,2,1
260985861	5096		3.340	69	1
261136679	5950	4.438	6.268	137	4,1
261867566	5565	4.463	3.739	25	12
263003176	6296	4.438	14.340	76	1,12,13
264678534	5052	4.580	16.191	42	18,19,20
264979636	5596	4.322	17.879	22	7
266980320	5586	4.368	6.036	24	1
267263253	6888	4.234	4.127	23	1
267489265	7851	4.170	1.551	24	14

Table 4. Continue.

TIC ID	T_{eff} (K)	$\log g$ (dex)	P_{orb} (days)	t_{SPAN} (days)	Sectors
267561446	3855	4.685	1.283	42	15,16
267574918	5780	4.438	1.408	70	19
268334473	5759	4.448	16.732	22	19,20
268644785	6003	4.170	3.329	41	7
268766053	4953	4.557	3.310	17	3
269450900	8269	3.930	2.324	21	13
269701147	5556	4.490	8.880/28.579	106	14,15,16,17,18,19,22
270341214	6409	4.201	14.192	48	1
270380593	4910	4.601	3.836	20	4
270468559	5743	4.141	4.642	17	8
270507305	5848	4.332	1.228	67	11
271168962	6030	4.094	5.322	18	11
271596225	3704	4.774	1.801/4.140	288	9,8,7,5,6,4,3,2,1
271596418	5670	4.166	0.556	288	5,6,4,3,2,1
271893367	5766	4.030	5.857	110	1
271971130	3075	4.438	19.288	286	9,8,7,5,6,4,3,2,1
272086159	3270	4.982	16.155	240	5,6,4,3,2
272635712	5711	4.240	12.717	89	16
273985865	5626	4.562	3.424	76	13,12,1
274138511	5280	4.445	2.774	22	7
274662200	3526	4.711	1.228	35	15,16
274762761	2972	5.157	1.033	28	14,15
275248683	3778	4.870	0.531	15	8
276128561	5636	4.372	3.288	18	11
277103955	4780	4.570	1.309	217	4
277507814	6588	4.186	0.617	47	15,16,17
277634430	3231	4.438	2.326	70	10
278348461	6509	4.172	5.453	17	14
278866211	6054	4.394	2.194	211	2,1

Table 4. Continue.

TIC ID	T_{eff} (K)	$\log g$ (dex)	P_{orb} (days)	t_{SPAN} (days)	Sectors
278895705	6169	4.242	8.760	267	9,8,5,6,4,3,2,1
279251651	4119	4.730	0.404	243	4
279740441	4305	4.570	0.742	59	3
279741379	4628	4.322	66.799	88	3,2,1
280095254	5454	3.442	10.090	70	13,6,2
280097543	4940		9.449	26	2
280206394	6446	4.379	11.237	45	10,9
280210963	5675	4.373	2.828	19	6
281459670	5943	4.425	3.174	46	2,1
281541555	5377	4.425	4.743	48	2,1
281575427	6223	4.060	4.252	49	2,1
281731203	5287	3.880	11.633	21	9
281781375	5605	4.400	43.829	49	2,1
281909674	5945	4.467	4.035	19	6
283474780	4876		3.994	17	17
284441182	3624	4.746	2.527	37	17
285048486	3907	4.623	3.492	22	20
286355915	6531	4.137	4.077	19	18
286865921	5510	4.441	4.971	20	10
287080092	6114	4.293	37.473	23	15,17,18,19
287139872	3652	4.714	0.935	22	14,15,16,17,18,19
287156968	5696	4.266	25.060	74	13,12,11
287225295	5493	4.520	0.610	26	21
287563610	5318	4.437	3.800	21	11
287776397	6090	3.299	2.392	134	13,12,11,10,6,3
288132261	6124	4.154	10.261	25	14,20
288636342	6554	4.243	17.734	22	19
288735205	4699	4.546	3.478	81	14,17,18
289535142	6621	4.207	2.338	17	8

Table 4. Continue.

TIC ID	T_{eff} (K)	$\log g$ (dex)	P_{orb} (days)	t_{SPAN} (days)	Sectors
289580577	5700	4.481	5.385	23	14,15,16,18,19
289793076	5523	4.522	3.044	23	1
290131778	6188	4.272	3.309	22	1
292321872	6322	3.770	8.667	20	18
294301883	6070	4.420	4.465	21	10
294395926	5624	4.391	11.317	60	9
294471966	5180	4.543	6.317	71	14,15,16
294780517	5107	4.544	15.650	219	9,8,7,5,6,4
294781547	5456	4.467	13.773	264	13,12,11,10,9,8,7,6,4,3,2,1
294981566	6734	4.186	1.915	213	13,11,10,9,8,7,5,6,4,3
296739893	3633	4.804	5.098	18	8
296780789	3404	4.911	13.577	18	8
298073824	6906	4.438	1.229	49	14,15
298666530	5780	4.438	0.573	22	20
299799658	5394	4.509	4.115	51	13,1
299945285	6270	4.075	52.392	243	9,8,7,5,6,4,3,2
300013921	5379	4.505	163.987	289	9,8,7,5,6,4,3,2,1
300038935	8208	4.260	29.049	288	13,12,11,10,9,8,7,5,6,4,3,2,1
300710077	3471	4.877	5.447	268	9,8,7,5,6,3,2,1
300810086	5071		0.668	96	2
300871545	6380	4.249	4.817	277	2,1
302773669	5925	4.100		42	18
302895996	3462	4.883	0.568	17	6
304042899	6746	4.416	12.442	45	10
305048087	3139	5.049	5.434	24	2
305424003	6272	3.840	4.585	24	12
306263608	5625	4.468	20.772	17	17
306362738	5600	4.429	2.782	19	6

Table 4. Continue.

TIC ID	T_{eff}	$\log g$	P_{orb}	t_{SPAN}	Sectors
	(K)	(dex)	(days)	(days)	
306472057	6572	4.354	139.311	176	9,8,5,6,4
306955329	5103	4.503	6.364	17	17
306996324	3806	4.736	8.243/15.656	21	10
307111282	5518	4.290		20	17,18
307210830	3469	4.940	2.253/3.691/7.451	156	12,11,10,9,8,5,2
308050066	6655	3.900	11.176	20	9
308994098	6988	4.256	99.774	128	11,10,9,8,4,1
309791156	4666	4.230	19.573	219	5,6,1
309792357	5350	4.523	33.268	281	3,2,1
311035838	5224	4.558	2.900	21	16
311121985	6375	4.000	1.357	23	18,19
313506357	6023	4.240	1.537	16	16,17
314865962	5493	4.430	22.454	134	6,3,2,1
315002523	6071	3.933	3.303	35	8
316916655	6805	4.260	2.874	23	5
316937670	3765	4.752	0.624	49	2,1
317060587	5958	4.340	9.140	51	13,1
317548889	6213	4.438	6.866	20	6
317597583	5504	4.580	12.053	39	17,18,19
318022259	3691	4.709	2.156/6.222	21	20
319259194	6308	3.987	70.365	137	13,12,11,9,8,5
320417762	9177	3.950	1.036	22	7
321041369	5672	4.510	1.538	22	19
321857016	5387	4.463	6.956	22	16
322063810	4020	4.438	3.516	25	2
322202434	5365	4.480	1.401	58	16,17,18
322270620	3614	4.813	12.959	51	13
323132914	5599	4.461	51.165	96	10,11,12,13

Table 4. Continue.

TIC ID	T_{eff}	$\log g$	P_{orb}	t_{SPAN}	Sectors
	(K)	(dex)	(days)	(days)	
326453034	5063	4.484	14.446	24	2
327301957	5206	4.631	13.926	26	13
332064670	5270	4.420	0.737	22	21
332477926	3849	4.657	16.217	23	14,15,16,17,18,19
333473672	5914	4.460	12.998	38	16,17
334305570	7199	4.359	16.604	21	10
335499997	5967	3.950	0.434	21	9
336732616	6351	4.229	3.548	23	1
339636032	6231	3.990	6.879	107	9,8,7,6
339672028	5760	3.977	10.331	108	13,10,9,7,6
339733013	5834	4.240	5.621	198	4
339857675	6280	4.260	3.514	61	9,8,7,6
343628284	3391	4.844	8.114	46	15,16
346418409	4993	4.669	2.756	20	16
348673213	3896	4.642	0.901	17	18
348755723	3267	4.438	4.504	17	8
348770361	5793		2.769	47	1
348844154	5493	3.920	29.174	73	4
349095149	5802	4.445	91.680	287	13,12,11,10,9,8,7,5,6,4,3,2,1
349373192	8658	3.920	0.770	74	5,6,4
349518800	5830	4.260	2.166	216	4
349790953	4997	2.360	1.552	207	8
349827430	6404	4.160	5.551	24	14,20
349829627	4997	3.452	6.487	239	13,11,10,9,8,7,5,6,4,3,1
350153977	5500	4.990	3.184	52	12
350332997	5623	4.375	1.917	46	11
350618622	6462	4.350	5.849/52.978	264	13,12,11,10,8,7,5,6,4,3,2,1
350743714	6038	3.960	7.762	229	3
351601843	4046	4.610	0.605	26	13

Table 4. Continue.

TIC ID	T_{eff}	$\log g$	P_{orb}	t_{SPAN}	Sectors
	(K)	(dex)	(days)	(days)	
352764091	5891	4.302	9.602	85	15
353475866	3474	4.772	1.767	21	19
353782445	6225	5.061	11.835	132	14,15,16,17,18,19
354594208	5904	4.310	0.867	18	17
355509914	4746	4.527	1.738	47	1,2
355703913	5380	4.434	2.106	47	1,2
355867695	4225	4.576	3.127/7.491	24	14
356158613	5780	4.648	2.369/24.710	36	14,15
356473034	5267	4.320	2.616	21	20
356978132	6499	4.354	60.187	23	14,15,16,17,18,19
358460246	5777	4.304	15.404	289	1,2,3,4,5,6
359271092	3766	4.760	7.576	44	9,10
359496368	4043	4.690	2.666	90	14,15,16,17,18,19
364107753	6059	4.290	3.905	26	12
364186197	6594	4.230	4.425	83	16,17,18,19
364393429	6282	4.378	2.628	289	1,2,3,4,5,6,7,8,9,10,11,12,13
365639282	3692	4.781	10.872	19	6
365690646	6963	4.147	12.983	20	6
365733349	6180	4.580	2.700	82	15,16,17,18
365938305	5396	4.505		25	14
366576758	5027	4.519	11.388	22	7
366622912	4973	4.438	3.115	21	7
366989877	6122	4.309	15.505	26	13
367366318	6768	4.100	2.735	21	19
367607434	4941		8.292	39	16,17,18,19
369327947	3194	4.967	2.029	51	12
369960846	5192	4.462	1.606	24	13
370133522	3325	4.887	0.518	26	13
371234684	6193	4.286	3.923	20	20

Table 4. Continue.

TIC ID	T_{eff} (K)	$\log g$ (dex)	P_{orb} (days)	t_{SPAN} (days)	Sectors
373424049	8688	4.322	0.963	45	9,10
374829238	3783	4.438	18.641	177	9,7,6,3,2
374997123	6082	4.333	10.194	271	13,12,11,10,9,7,5,6,4,3,2,1
375059587	5854	4.221	12.669	271	9,7,5,6,4,3,2,1
375506058	7400	4.110	2.650	44	15,16
377064495	5391	4.525	0.447/10.781/16.372	17	8
377191482	4998		2.956	22	14,15,16,17
377293776	3407	4.761	2.044	112	14,15,16
379240073	6519	4.221	3.164	25	13
380589029	6346	4.385	1.348	23	13
381976956	4866	2.506	22.339	287	5,6,4,3,2,1
381979901	6102	4.286	3.254	47	13
382188882	6366	4.162	4.801	166	3
382437043	6516	3.994	14.642	286	13,12,11,10,9,8,7,5,6,4,3,2,1
382626661	5250	4.642	17.618	290	13,12,11,10,9,8,7,5,6,4,3,2,1
386435344	6529	4.003	16.597	18	8
387527558	3514	4.814	3.624	38	18
387690507	3688	4.782	6.388	19	6
387834907	5195		12.640	60	16,17
388076005	5932	4.480	1.712	21	16,18
388104525	5650	4.289	2.500	123	4,3,2,1
388106759	5705	4.092	28.304	286	9,8,7,5,6,4,3,2,1
389924075	5909	4.262	105.585	245	12,11,10,9,8,7,5,6,4,2,1
391904697	5249	4.684	47.024	284	5,6,4,3,2,1
393414358	5570	4.011	4.378	39	6
394137592	5479	3.770	11.535	23	1
394698182	5768	4.310	3.712	49	1

Table 4. Continue.

TIC ID	T_{eff} (K)	$\log g$ (dex)	P_{orb} (days)	t_{SPAN} (days)	Sectors
396562848	3414	4.973	1.949	42	18
396720998	50000	5.803	32.380	62	5,4,3
396740648	5058	4.539	3.770	21	19,20
398733009	31000	5.600	0.818	19	4
399144800	6270	4.545	27.214	47	11,10
402026209	5436	4.460	1.338	22	2
403224672	5795	4.438	1.008	24	1
403693875	3965	4.686	3.524	19	6
404340025	6783	4.243	2.676	20	11
405454160	5383	4.424		18	8
406672232	5098	4.547	1.021	18	14
406941612	3566	4.835	4.679	51	12
407126408	4948	4.604	11.094	51	12
407966340	6337	4.438	7.049	24	5
408159788	5747	4.570	2.301	24	5
408203470	3446	4.839	0.581	31	15
408310006	6313	4.326	5.444	17	8
409934330	8048	4.438	2.489	25	13
410094645	7341	4.142	3.330	17	8
410153553	3043	5.097	0.463	23	1
410245915	6173	4.220	0.989	18	8
410450228	7447	3.790	15.778	39	9
413248763	3505	4.906	3.931	18	8
413376180	5227	4.474	1.354	19	10
415969908	3644	4.799	11.666	24	2
416195870	5040	4.385	2.744	108	14,15,16,17
417676622	5875	4.265	5.401	49	14,15
417705690	5420	4.380	2.362	23	18,19
417931607	5781	4.431	16.538	49	14,15

Table 4. Continue.

TIC ID	T_{eff} (K)	$\log g$ (dex)	P_{orb} (days)	t_{SPAN} (days)	Sectors
417948359	4973	4.540	3.316	45	15,16
418959198	4528	4.483	4.898	21	16
420049884	5205	4.459	4.107	21	4
420112587	3212	4.980	11.063	22	14,15,16,17,19
420112589	3248	4.954	11.064	111	14,15,16
421894914	6124	4.380	5.308	51	13,1
422655579	6059	3.923	2.903	19	4
422756130	3575	4.723	3.131	42	19
423275733	6010	4.133	2.053	16	8
424391516	6311	4.378	11.592	23	14,15,16,17,18,19
424865156	6532	3.968	2.205	44	14,15
425206121	7346	4.142	4.612	21	7
425934411	3658	4.438	0.853	45	2,1
425997655	4813	4.380	3.976/12.161/17.668/29.797	110	4,3,2,1
427348923	4425	4.570	4.731	19	6
427654774	3453	4.953	5.223	39	17,18
428679607	5550	4.370	2.679	22	20
429304876	5085	3.920	6.839	20	9
429358906	3331	4.950	16.047	21	10
430677414	7960	4.230	0.467	35	16,17
431514478	10012	4.299	8.495	18	17
431999925	3266	4.985	1.445	19	7
432008938	3359	4.935	9.653	39	8
434486077	5156	4.468	2.228	20	9
437242640	5700	4.506	4.318	21	9
437248515	6302	4.309	3.406	20	9
437333618	5715	4.343	4.298	18	11

Table 4. Continue.

TIC ID	T_{eff}	$\log g$	P_{orb}	t_{SPAN}	Sectors
	(K)	(dex)	(days)	(days)	
438490744	3021	5.107	1.666	16	6
439456714	3748	4.757	3.994	17	3
440100539	5891	4.300	12.602	18	17
440777904	6373	4.273	3.355	20	7
441462736	5105	3.392	14.279	24	2
441739020	6453	5.200	40.731	87	15,16,18,19,20
441739871	3520	4.761	3.798	23	14,15,16,17,18,19
444842193	5741	4.471	1.078	45	9
445822015	4841	4.710	1.664	19	9
445859771	5736	4.390	4.631	23	15
447061717	3535	4.849	24.246	45	10,9
451599528	5962	4.200		51	13,12
451606970	5262	3.980	38.361	52	13,12
452808876	6087	3.910	2.706	21	5
452866790	3332	4.915	1.198	21	7
453211454	5560	4.438	18.120	22	7
453260209	3751	4.757	1.213	70	12,11,10
455096220	6096	4.215	3.647	21	7
455135327	6304	4.359	2.811	21	7
457138169	6273	4.200	1.093	25	21
458478250	5787	4.500	2.255	84	14,15,16,17
459942762	5998		0.586	24	5
459969957	4968	4.500	19.318	106	14,15
459978312	5000		23.288	128	14,15,16,17
460984940	5849	4.530	2.797	47	11,10
461662295	5326	4.430	10.256	24	20
466840711	6933	4.251	2.485	44	11
467179528	3618	4.794	10.895/18.795	48	14,15
467666275	6711	4.064	1.381	47	11,10

Table 4. Continue.

TIC ID	T_{eff} (K)	$\log g$ (dex)	P_{orb} (days)	t_{SPAN} (days)	Sectors
468148930	5818	4.338	3.717	24	13
468880077	5175	4.580	5.808	24	5
468987719	5645	4.377	3.333	21	7
470381900	3181	4.948	2.501	22	19
470987100	3876	4.624	4.121	23	20
1400770435	5941	4.230	13.743	130	14,15,16,17,18,19
1551345500	4415	4.698	47.387	23	14,15,16,17,18,19